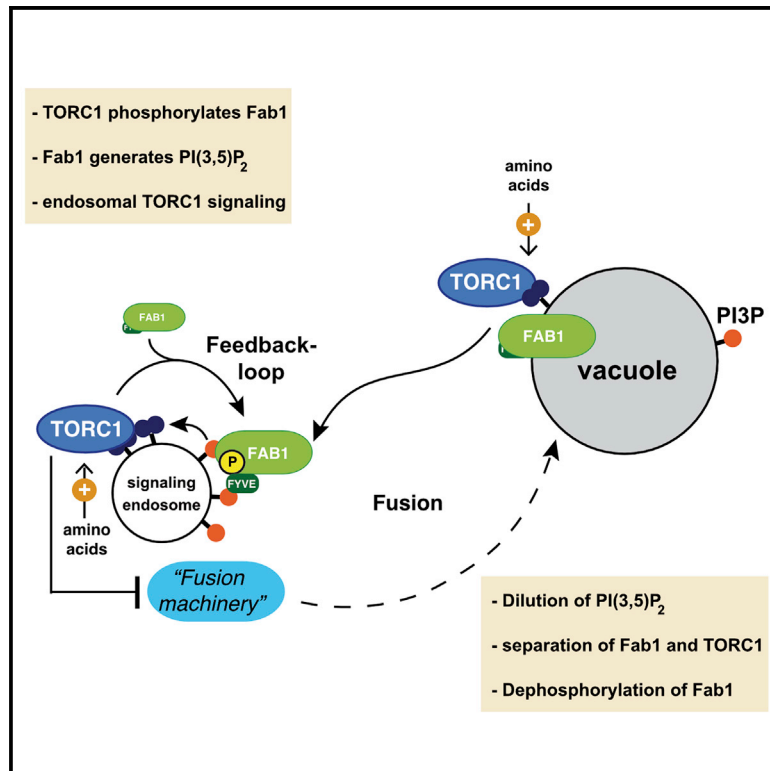# TORC1 Determines Fab1 Lipid Kinase Function at Signaling Endosomes and Vacuoles

Graphical Abstract

Authors

Zilei Chen, Pedro Carpio Malia, Riko Hatakeyama, ..., Jörn Dengjel, Claudio De Virgilio, Christian Ungermann

Correspondence

claudio.devirgilio@unifr.ch (C.D.V.), cu@uos.de (C.U.)

In Brief

Chen, Malia, Hatakeyama, et al. demonstrate that the yeast Target of Rapamycin Complex 1 (TORC1) phosphorylates the lipid kinase Fab1, a homolog of metazoan PIKfyve. Fab1 phosphorylation shifts both complexes from the vacuole to signaling endosomes and changes TORC1 activity, suggesting a regulatory feedback loop in cellular signaling from these organelles.

Highlights

- The Fab1 lipid kinase is a substrate of the Target of Rapamycin Complex 1 (TORC1)

- Fab1 and TORC1 localize to signaling endosomes and the vacuole

- Fab1 phosphorylation shifts TORC1 to signaling endosomes and changes its activity

- Fab1 and TORC1 function in a regulatory feedback loop, which controls signaling

Article

TORC1 Determines Fab1 Lipid Kinase Function at Signaling Endosomes and Vacuoles

Zilei Chen,[1,6] Pedro Carpio Malia,[1,6,7,8] Riko Hatakeyama,[2,6,9] Raffaele Nicastro,[2] Zehan Hu,[2] Marie-Pierre Péli-Gulli,[2] Jieqiong Gao,[1] Taki Nishimura,[3] Elja Eskes,[4] Christopher J. Stefan,[3] Joris Winderickx,[4] Jörn Dengjel,[2] Claudio De Virgilio,[2,*] and Christian Ungermann[1,5,10,*]

[1]Department of Biology/Chemistry, Biochemistry Section, University of Osnabrück, Barbarastrasse 13, 49076 Osnabrück, Germany
[2]Department of Biology, University of Fribourg, Chemin du Musée, CH-1700 Fribourg, Switzerland
[3]MRC Laboratory for Molecular Cell Biology, University College London, Gower Street, London WC1E 6BT, UK
[4]Functional Biology, KU Leuven, Kasteelpark Arensberg 31, 3000 Leuven, Belgium
[5]Center of Cellular Nanoanalytics Osnabrück (CellNanOs), University of Osnabrück, Barbarastrasse 11, 49076 Osnabrück, Germany
[6]These authors contributed equally
[7]Present address: Department of Molecular Metabolism, Harvard School of Public Health (P.C.M.), Boston, MA 02115, USA
[8]Present address: Department of Cell Biology, Harvard Medical School, Boston, MA 02115, USA
[9]Present address: Institute of Medical Sciences (RH), School of Medicine, Medical Sciences & Nutrition, University of Aberdeen, Foresterhill, Aberdeen AB25 2ZD, UK
[10]Lead Contact
*Correspondence: claudio.devirgilio@unifr.ch (C.D.V.), cu@uos.de (C.U.)
https://doi.org/10.1016/j.cub.2020.10.026

SUMMARY

Organelles of the endomembrane system maintain their identity and integrity during growth or stress conditions by homeostatic mechanisms that regulate membrane flux and biogenesis. At lysosomes and endosomes, the Fab1 lipid kinase complex and the nutrient-regulated target of rapamycin complex 1 (TORC1) control the integrity of the endolysosomal homeostasis and cellular metabolism. Both complexes are functionally connected as Fab1-dependent generation of $PI(3,5)P_2$ supports TORC1 activity. Here, we identify Fab1 as a target of TORC1 on signaling endosomes, which are distinct from multivesicular bodies, and provide mechanistic insight into their crosstalk. Accordingly, TORC1 can phosphorylate Fab1 proximal to its PI3P-interacting FYVE domain, which causes Fab1 to shift to signaling endosomes, where it generates $PI(3,5)P_2$. This, in turn, regulates (1) vacuole morphology, (2) recruitment of TORC1 and the TORC1-regulatory Rag GTPase-containing EGO complex to signaling endosomes, and (3) TORC1 activity. Thus, our study unravels a regulatory feedback loop between TORC1 and the Fab1 complex that controls signaling at endolysosomes.

INTRODUCTION

Eukaryotic organelles differ in the lipid and protein composition of their surfaces and thus maintain a unique identity. Along the endomembrane system, proteins are transported by vesicles that are generated at the donor compartment and fuse with an acceptor organelle. Despite this active transport between organelles, each organelle maintains its identity. Apart from the fusion and fission machineries involved in each transport step, organelle-specific phosphatidylinositol phosphates (PIPs) are important markers that contribute to the identity of distinct organelles.[1] PIPs are phosphorylated derivatives of phosphatidylinositol (PI), which can be modified at three positions by specific lipid kinases and phosphatases to generate seven distinct isoforms.[2] Organelle-specific PIPs are proposed to recruit specific proteins to their surface, which then have decisive roles in cell signaling, membrane trafficking, and lipid metabolism. Proteins may recognize not only PIPs but additionally also membrane-associated proteins, which increases the specificity of their

localization—a mechanism termed coincidence detection. Consequently, PIP production and turnover is tightly controlled to maintain organelle identity.[2]

Within the endosomal system, proteins and lipids are transported either from the plasma membrane or Golgi to the early endosome. These endosomes then undergo maturation and sorting processes, whereby a number of membrane proteins are sorted into intraluminal vesicles by the endosomal sorting complexes required for transport (ESCRT) machinery, whereas others are recycled with the support of retromer complexes. ESCRTs function in consecutively acting complexes on endosomes. Early acting complexes (0–II) recognize ubiquitinated membrane proteins, whereas ESCRT-III and the interacting ATPase Vps4 corral the proteins and promote formation of intraluminal vesicles.[3] Mature late endosomes, also called multivesicular bodies (MVBs), eventually fuse with the lysosome.[4] Two PIPs, phosphatidylinositol-3-phosphate (PI3P) and phosphatidylinositol-3,5-bisphosphate ($PI(3,5)P_2$), are essential for endosomal and lysosomal biogenesis. The Vps34 kinase complex II

produces PI3P at endosomes, which is also found at vacuoles in yeast (or lysosomes in metazoan cells).[2,5] Subunits of both the retromer and ESCRT complexes have PX and FYVE domains, which bind specifically to PI3P and thus endosomes.[6] PI3P can be further phosphorylated to the low abundant $PI(3,5)P_2$, which is strongly upregulated during osmotic stress.[7] In yeast, osmotic stress results in fragmentation of the vacuole to maintain organelle integrity.[8] Vacuolar fragmentation is also required for the inheritance of vacuoles to daughter cells, and also here $PI(3,5)P_2$ levels play an important regulatory role.[9] Moreover, nutrient supply as an activator of TORC1 also affects vacuole fragmentation,[10] though the TORC1 substrate(s) that is relevant for this process remains unknown.

The PI3P 5-kinase Fab1, called PIKfyve in metazoans, is part of a multisubunit complex, which includes the $PI(3,5)P_2$ phosphatase Fig4, the scaffold protein Vac14, and Atg18.[1,11–13] Fab1, Fig4, and Vac14 form the core of the complex.[11,13,14] Full Fab1 activity in yeast also requires the vacuolar membrane protein Vac7[15] and is controlled by Atg18.[16,17] Consequently, mutants lacking either Fab1, Vac7, or Vac14 exhibit very large vacuoles and defects in protein sorting at endosomes and vacuoles.[18–21] Likewise, inactivation of metazoan PIKfyve affects $PI(3,5)P_2$ production and lysosomal biogenesis and homeostasis.[1,22–24] In humans, such mutations result in devastating neurodegenerative diseases, demonstrating that $PI(3,5)P_2$ levels need to be tightly controlled.[25–28]

The identification of $PI(3,5)P_2$ effectors starts to shed light on the role of this lipid in lysosomal biogenesis and homeostasis. In yeast, the most prominent interactor is Atg18,[16] which can directly induce membrane fragmentation.[29] Additional $PI(3,5)P_2$-interactors include lysosomal ion channels, the vacuolar ATPase, and a subunit of the lysosomal target of rapamycin complex 1 (TORC1).[1,7,12,23,30–33]

TORC1 was initially identified in yeast, and is conserved across eukaryotic species.[34] It consists of the protein kinases Tor1 or Tor2 (mTOR in humans), Kog1/Raptor, Lst8/mLST8, and the yeast-specific subunit Tco89.[34] TORC1 is a cellular pacemaker that promotes anabolic processes and growth. Nutrients, particularly amino acids, are required for TORC1 activity.[35] Amino acids are sensed by another conserved lysosomal complex, the Rag GTPase-containing EGO complex (Ragulator-Rag complex in metazoans) and its regulators, such as the SEACIT and SEACAT complexes (GATOR1 and 2 in metazoans).[36–38] The FYVE domain-containing yeast protein Pib2 represents another amino acid-sensing branch that regulates TORC1, although its conservation in higher eukaryotes has not been demonstrated.[39–43] Recent data suggest that yeast TORC1 also responds to glucose as it oligomerizes upon glucose starvation in structures known as TORC1 bodies or TOROIDs, in which TORC1 is inactive.[44,45] Inactivation of TORC1 in turn activates catabolic processes including autophagy, highlighting its central function in growth control.

The EGO complex and TORC1 localize to a special endosomal population in yeast that we coined "signaling endosomes."[46,47] Such endosomes are distinct from previously described metazoan endosomes involved in signaling via, for instance, the epidermal growth factor.[48] Ivy1, an effector of the vacuolar Rab GTPase Ypt7[49] and inhibitor of the Fab1 complex[50] colocalizes with Fab1 and the EGO complex to dots proximal to the vacuole.[49,51]

We now present evidence that signaling endosomes have a key function in endosome and vacuole membrane homeostasis. Ivy1, Fab1, the EGO complex, and TORC1 all localize to signaling endosomes in addition to their vacuolar localization. We uncover that Fab1 is a TORC1 substrate and that phosphorylation of Fab1 shifts not only the primary localization of the Fab1 complex from vacuoles to signaling endosomes but also of TORC1. This in turn results in a local $PI(3,5)P_2$ accumulation at signaling endosomes and altered TORC1 activity. Our data highlight a novel feedback loop between a lipid kinase and the metabolically regulated TORC1 at endomembranes.

RESULTS

TORC1 and Fab1 Localize to Signaling Endosomes and Interact with Each Other

Both Ivy1, as a Fab1 inhibitor, and TORC1 localize to the vacuole and distinct dots.[49–51] As Ivy1 localization was unaffected by ESCRT-III deletions,[49] we previously discarded the possibility that Ivy1 resides also on endosomes. However, it was recently shown that a second population of endosomes exists, which contains an endosomal pool of TORC1 and the EGO complex.[52] As Ivy1 also strongly colocalizes with EGO components in dots proximal to the vacuole,[49] we wondered if all proteins, including TORC1 and Fab1, function together on signaling endosomes.

To ask if Ivy1, Fab1, and TORC1 are present on these endosomes, we analyzed the localization of GFP-tagged Ivy1 relative to mCherry-tagged Kog1 (a subunit of TORC1), Vps4 (the disassembling ATPase of ESCRT-III proteins at MVBs), and Vps8 (a subunit of endosomal CORVET, which binds the Rab5-like Vps21 protein). Indeed, we observed that a fraction of Ivy1 colocalized with Kog1 and Vps8 positive dots but not with dots positive for Vps4 (Figures 1A and 1B). This suggests that a significant portion of Ivy1 is present on signaling endosome, but not MVBs, together with the endosomal TORC1.
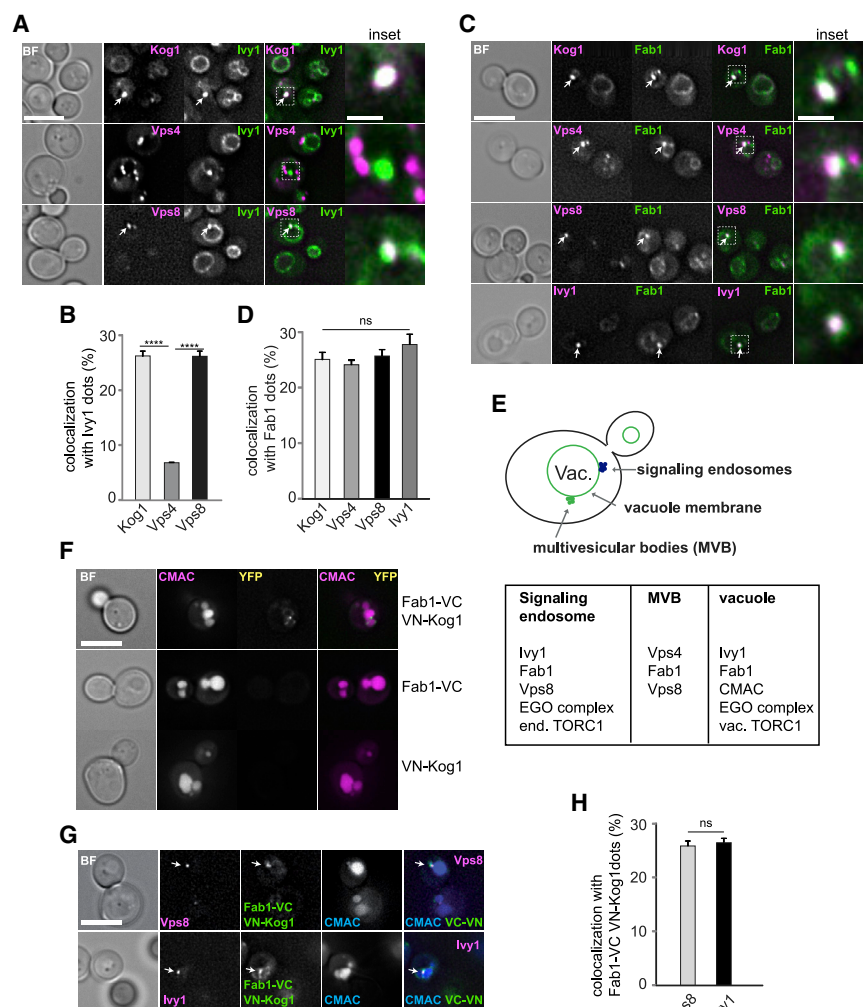
We then analyzed if Fab1 is also present on these signaling endosomes with Ivy1 and TORC1. Indeed, a significant amount of mNeonGreen-tagged Fab1 colocalized with mCherry-tagged Kog1, Ivy1, and Vps8 in dots proximal to the vacuole (Figures 1C–1E). Fab1 was, however, also present on Vps4-positive MVBs, and thus has a broader distribution (Figures 1C–1E).

To determine if TORC1 and Fab1 contact each other on signaling endosomes, we added the C-terminal half of the Venus fluorescence protein to Fab1 (VC) and the N-terminal half to Kog1 (VN). If close enough, both halves (VN and VC) will interact and form a fluorophore. We detected fluorescent dots proximal to vacuoles (Figure 1F), which colocalized with Vps8 and Ivy1 (Figures 1G and 1H), and this signal was specific as Fab1-VC alone or co-expression with Vac8-VN did not produce any signal (Figure 1F).

Overall, our data reveal that Ivy1, Fab1, and TORC1 localize both to vacuoles and to signaling endosomes (Figure 1E), where Fab1 and TORC1 are in close proximity.

Fab1 Is Phosphorylated by TORC1

As Fab1 and TORC1 are in close proximity on signaling endosomes, we asked whether Fab1 is a direct target of TORC1 and thus conducted two lines of independent assays. As a first approach, we compared the phosphoproteome of yeast strains

Figure 1. A Pool of Fab1 Complex Localizes with TORC1 to Signaling Endosomes

(A) Ivy1 is a marker of signaling endosomes. Cells expressing Ivy1-mGFP and mCherry-Kog1 (under the *ADH1* promoter), Vps4-3xHA-mCherry, or Vps8-mCherry were imaged by fluorescence microscopy. Scale bar, 5 μm. Scale bar (inset), 1 μm.

(B) Quantification of colocalization of Ivy1-positive dots with Kog1, Vps4, or Vps8 dots. The percentage of colocalization normalized to the number of Ivy1-dots was plotted. At least 150 cells and 60 Ivy1 dots were counted from three independent experiments. Results are means ± standard deviation (SD). Significance was determined with a two-tailed Student's t test (****p < 0.0001).

(C) Fab1 localizes to the vacuole, signaling endosomes, and MVBs. Cells expressing Fab1-mNeonGreen and mCherry-Kog1 (under the *ADH1* promoter), Vps4-3xHA-mCherry, Vps8-mCherry, or Ivy1-mCherry were imaged by fluorescence microscopy. Scale bar, 5 μm. Scale bar (inset), 1 μm.

(D) Quantification of colocalization of Fab1-positive dots with Kog1, Vps4, Vps8, or Ivy1 dots. Fab1 dots colocalizing with mCherry signal were counted and plotted as percent of the total number of Fab1 dots. At least 150 cells and 60 Fab1 dots were counted from three independent experiments. Results are means ± SD; ns, no significant difference.

(E) Summary of Fab1 localization in yeast cells. The table summarizes markers of signaling endosomes, MVBs, and vacuoles.

(F) Proximity of TORC1 and Fab1 by bimolecular fluorescence complementation assay. Fab1 was C-terminally tagged with the C-terminal half of the Venus fluorescence protein (VC), and Kog1 was N-terminally tagged with N-terminal half (VN) under the control of the *CET1* promoter. Cells were monitored by fluorescence microscopy. Scale bar, 5 μm.

(G) Fab1 and TORC1 interact at signaling endosomes. Cells co-expressing VN-Kog1 and Fab1-VC were co-expressed with Vps8-mkate (top) or Ivy1-mkate (bottom) and stained with CMAC. Analysis was done as in (A). Scale bar, 5 μm.

(H) Quantification of colocalization between Fab1-TORC1 dots and Vps8 or Ivy1 dots. The percentage of colocalization was calculated by counting colocalization dots divided by the total Fab1-VC VN-Kog1 dots. At least 150 cells and 50 dots were counted in each of the three independent experiments. Results are means ± SD; ns, no significant difference.

in the absence and presence of rapamycin, a TORC1 inhibitor, and identified serine residue 208 (Ser^{208}) in Fab1 as a potential target of TORC1 *in vivo*, whereas other sites in Fab1 (Ser^{125} and Ser^{155}) were unaffected. The same assay also identified the known bona fide TORC1 target residue Thr^{723} in Sch9 (Figure 2A).[53] Ser^{208} is located next to the PI3P interacting FYVE domain in Fab1 (residues 230–320; Figures 2A and 2B). In a second approach, we subjected Fab1 to *in vitro* TORC1 kinase assays in the absence or presence of wortmannin, a potent TORC1 inhibitor.[53,54] To this end, we expressed (in bacteria) and purified four overlapping His-tagged Fab1 fragments that covered the entire length of the protein and incubated them with purified TORC1 (from yeast) and radioactive [^{32}P]-ATP (Figure 2C). Autophosphorylation of Tco89 by TORC1 served as positive control for TORC1 activity. Of the four fragments, TORC1 only phosphorylated the N-terminal Fab1$^{1–600}$ construct in the absence, but not in the presence, of wortmannin

(Figure 2C). We confirmed via mass spectrometry that Fab1$^{1–600}$ was phosphorylated by TORC1 at Ser^{208}, Ser^{204}, and Ser^{210} (Figure 2A). Recombinant variants of Fab1$^{1–600}$, in which these three residues alone (3A) or combined with the adjacent Ser^{201} and Thr^{206} (5A), were mutated to alanines (Ala) (Figure 2B), were only marginally phosphorylated by TORC1 (Figure 2D). Based on these results, we conclude that TORC1 phosphorylates Fab1 at mainly Ser^{204}, Ser^{208}, and Ser^{210}.

Fab1 Phosphorylation Affects Vacuole Morphology and EGO Localization

To determine whether Fab1 phosphorylation by TORC1 affected endosome and vacuole biogenesis, we generated (using CRISPR/Cas9 gene editing) *fab1^{6A}* and *fab1^{6D}* mutant alleles. Here, the entire cluster of Ser/Thr residues between Ser^{202} and Ser^{210} was replaced by either Ala or phosphomimetic aspartates (Figure 2B). We initially analyzed strains expressing Fab1-
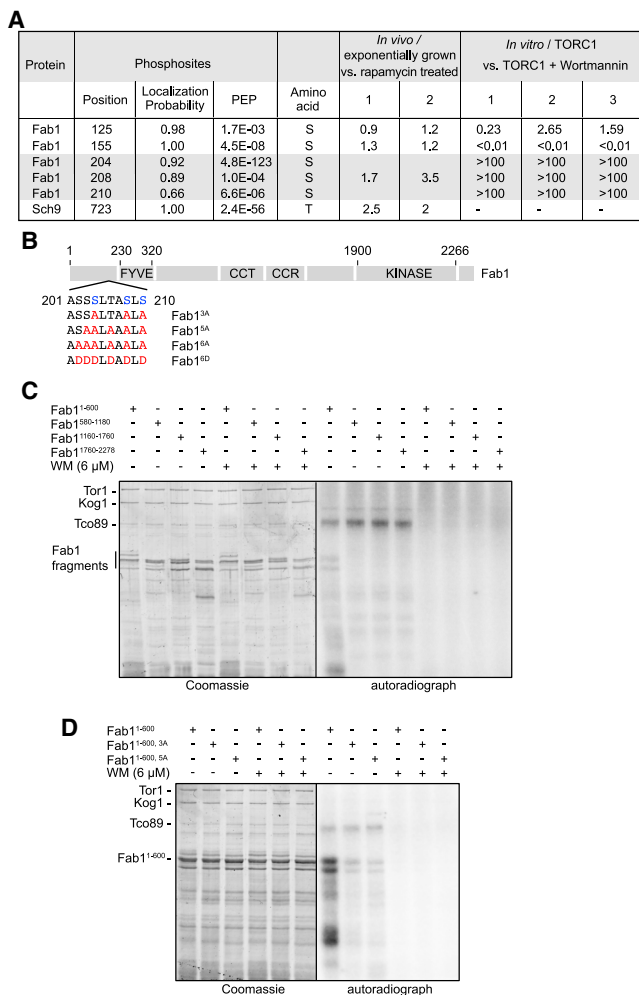
A

Protein	Phosphosites				In vivo / exponentially grown vs. rapamycin treated		In vitro / TORC1 vs. TORC1 + Wortmannin		
	Position	Localization Probability	PEP	Amino acid	1	2	1	2	3
Fab1	125	0.98	1.7E-03	S	0.9	1.2	0.23	2.65	1.59
Fab1	155	1.00	4.5E-08	S	1.3	1.2	<0.01	<0.01	<0.01
Fab1	204	0.92	4.8E-123	S			>100	>100	>100
Fab1	208	0.89	1.0E-04	S	1.7	3.5	>100	>100	>100
Fab1	210	0.66	6.6E-06	S			>100	>100	>100
Sch9	723	1.00	2.4E-56	T	2.5	2	-	-	-

B

C

D

Figure 2. TORC1 Phosphorylates Fab1

(A) TORC1 phosphorylates multiple residues within the N-terminal part of Fab1. The table shows the rapamycin sensitivity of phosphorylation of Ser[125], Ser[155], Ser[208] on Fab1, and Thr[723] of Sch9 *in vivo*, as detected by SILAC mass spectrometric analysis, and the identification of the phosphopeptide containing phosphorylated Ser[125], Ser[155], Ser[204], Ser[208], and Ser[210] detected on purified Fab1[1–600] following *in vitro* phosphorylation by TORC1. Wortmannin (WM) was used to inhibit TORC1 *in vitro* (see STAR Methods). PEP, posterior error probability; the smaller the number, the better is the hit. >100 implies that the phosphorylation levels of the respective amino acid residues were at least two orders of magnitude higher in samples treated with TORC1 when compared to the ones treated with TORC1 in the presence of WM.

(B) Model of the Fab1 sequence including the potential TORC1 target phosphosites. The Fab1 domains are indicated as FYVE domain (230–320), chaperonin containing TCP1 (CCT) domain (766–1039), conserved cysteine rich (CCR) domain (1181–1500), and kinase domain (1900–2266). The region between residues 201 and 210 is highlighted with the identified Ser[204], Ser[208], and Ser[210] shown in blue, the corresponding mutant alleles are indicated in red.

(C) TORC1 kinase predominantly phosphorylates the N-terminal part (encompassing amino acids 1–600) of Fab1. Purified recombinant His₆-Fab1 fragments (His₆-Fab1[1–600], His₆-Fab1[580–1180], His₆-Fab1[1160–1760], and His₆-Fab1[1760–2278]) were subjected to *in vitro* phosphorylation by TORC1 (purified from yeast) in the absence (−) or presence (+) of the TORC1 inhibitor WM (see STAR Methods). Representative SYPRO Ruby staining and autoradiography (^{32}P) blots are shown.

(D) Mutation of identified phosphosites strongly impairs the *in vitro* Fab1 phosphorylation by TORC1. Purified recombinant His₆-Fab1[1–600] containing,

mNeonGreen variants to trace their localization. While the wild-type Fab1 and Fab1[6A] protein localized mainly to round, wild-type-like vacuoles and to some dots, Fab1[6D] was enriched in dot-like structures around fragmented vacuoles (Figures 3A and 3B), which we identified as endosomes, as they colocalize with the endosomal Vps8 protein (Figure 6A). Interestingly, mCherry-tagged Ivy1 and the TORC1 subunit Kog1 showed a similar subcellular distribution pattern as Fab1, Fab1[6A], or Fab1[6D] in each of the strains expressing the respective Fab1 allele (Figures 3C–3E). Moreover, the EGO complex subunit Ego1 also colocalized with Kog1 in wild type, *fab1[6A]*, and *fab1[6D]* mutant cells (Figure 3D). Fab1[6D], however, did not colocalize with the MVB-marker Vps4 (Figures 3F and 3G; see inset), indicating that a fraction of Fab1[6D] accumulates on signaling endosomes. Finally, Fab1[6D]-expressing cells exhibited a significantly higher number of Ivy1, Ego1, and Kog1 dots next to vacuoles than wild-type cells or, even more, than Fab1[6A]-expressing cells (Figure 3H). These data indicate that Fab1 phosphorylation results in a significant shift of Fab1, TORC1, and the EGO complex from their vacuole localization to signaling endosomes. If, however, Fab1 cannot be phosphorylated, TORC1 and the EGO complex seem to become more confined to the vacuole, though some dot-like structures remain.

We next asked if the phosphomimetic *fab1[6D]* mutant, which showed an aberrant vacuole morphology, has defects in vacuole biogenesis or endolysosomal protein trafficking. As the vacuolar fragmentation observed in *fab1[6D]* cells can be the result of either increased fission or impaired fusion,[29] we stained vacuoles with FM4-64 and subjected cells to a brief incubation in water, which promotes vacuole fusion. Under these circumstances, the vacuoles in the *fab1[6D]* strain looked like the ones in wild type, suggesting that vacuole fragmentation in the *fab1[6D]* mutant is not due to defects in fusion (Figure S1A). Vacuole fragmentation often indicates defects in vacuole protein sorting and biogenesis, and *fab1Δ* cells also have an endosomal protein sorting defect.[21] Therefore, we tested the trafficking of selected cargo proteins from the Golgi or plasma membrane to the vacuole. Sorting of carboxypeptidase Y (CPY) to vacuoles as monitored by its abundance in cells was functional in wild-type and *fab1* mutants but defective if vacuole biogenesis was impaired by deleting the HOPS subunit Vps39 (Figure S1B). Likewise, trafficking of the plasma membrane localized dicarboxylic acid transporter Dip5 or carboxypeptidase S (Cps1) via MVBs into the vacuole lumen was unaffected in *fab1* mutants but impaired if the ESCRT protein Vps4 was lacking (Figures S1C and S1D). Similarly, a synthetic AP-3 cargo[55] was sorted efficiently to vacuoles in both *fab1* mutants but was missorted in a mutant lacking the AP-3 subunit Apl5 (Figure S1E). We thus conclude that phosphorylation of Fab1 results in both vacuole fragmentation and redistribution of Fab1 as well as the EGO complex and TORC1 components to signaling endosomes. However, it does not impair overall endocytosis or MVB biogenesis.

---

or not, the Ser-to-Ala mutations at positions Ser[204], Ser[208], and Ser[210] (3A), or at Ser[203], Ser[204], Ser[206], Ser[208], and Ser[210] (5A) were subjected to *in vitro* phosphorylation by TORC1 (purified from yeast) in the absence (−) or presence (+) of the TORC1 inhibitor WM. Representative SYPRO Ruby staining and autoradiography (^{32}P) blots are shown.
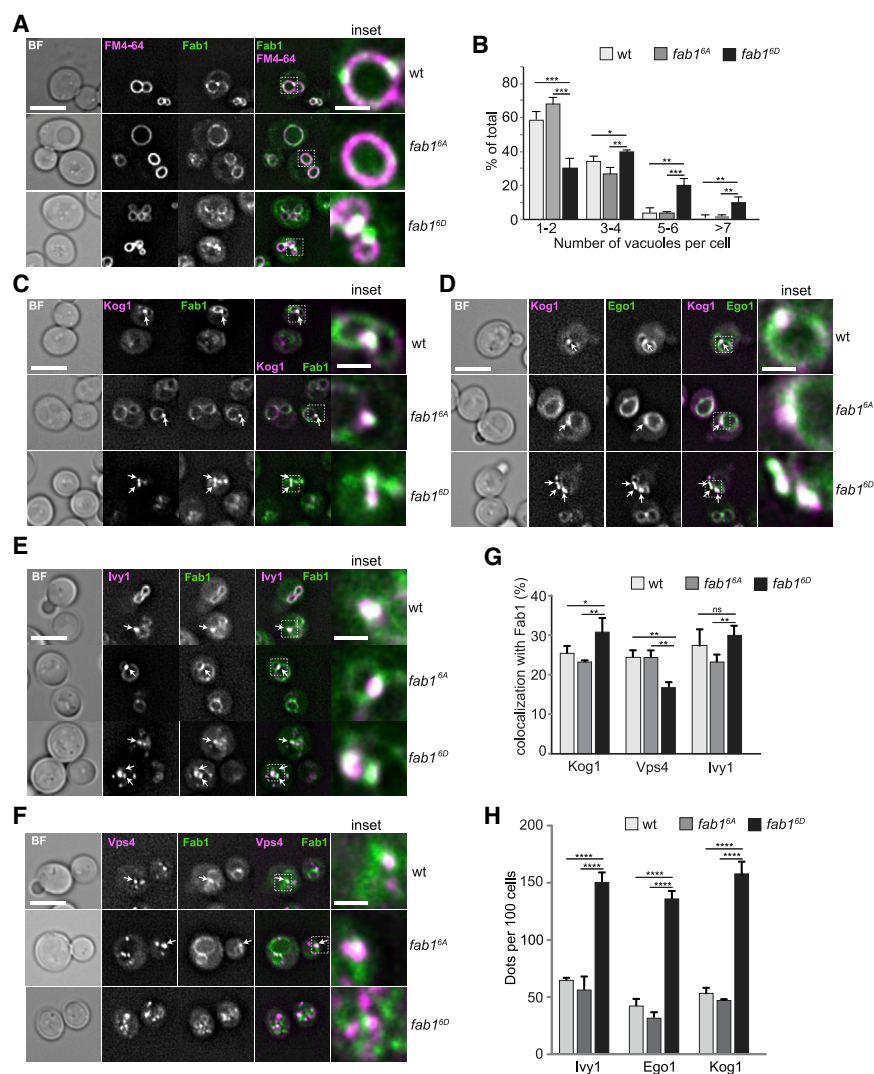
Figure 3. Phosphorylation Mutants of Fab1 Affect Fab1 Localization at Vacuoles and Endosomes

(A) Localization of Fab1 phosphomutants in cells. Fab1 was C-terminally tagged with mNeonGreen, and the Fab1[6A] and Fab1[6D] mutations were generated in the genome by CRISPR/Cas9 (see STAR Methods). Fab1 localization relative to FM4-64 stained vacuolar membranes was analyzed by fluorescence microscopy. Scale bar, 5 μm. Scale bar (inset), 1 μm.

(B) Quantification of vacuole morphology from (A). At least 200 cells were counted from three independent experiments. Results are means ± SD. Significance was determined with a two-tailed Student's t test (***p < 0.001; **p < 0.01; *p < 0.05).

(C) Kog1 localization in *fab1* mutants. Cells expressing Fab1-mNeonGreen with mCherry-Kog1 were analyzed by fluorescence microscopy. Scale bar, 5 μm. Scale bar (inset), 1 μm.

(D) Localization of Ego1 and Kog1 proteins in *fab1* mutants. Ego1 was tagged C-terminally with GFP, and Kog1 was tagged N-terminally with mCherry under the control of the *ADH1* promoter. All images were taken by fluorescence microscopy. Scale bar, 5 μm. Scale bar (inset), 1 μm.

(E and F) Ivy1 and Vps4 localization in *fab1* mutants. Ivy1-mCherry (E) or Vps4-3HA-mCherry (F) was co-expressed with Fab1-mNeonGreen, and analysis was as in (C).

(G) Quantification of colocalization between Fab1 and Kog1, Vps4, or Ivy1 dots in *fab1* mutants. Fab1 dots colocalizing with mCherry signal were counted and plotted as percent of total number of Fab1 dots. At least 60 Fab1 dots were counted in each of the three independent experiments. Results are means ± SD. Significance was determined with a two-tailed Student's t test (**p < 0.01; *p < 0.05; ns, no significant difference).

(H) Quantification of dot-like structures in (C–E). At least 100 cells were counted from three independent experiments. Results are mean ± SD. Significance was determined with a two-tailed Student's t test (****p < 0.0001).

See also Figure S1.

Fab1 Mutations Affect TORC1 Activity

TORC1 requires PI(3,5)P$_2$ on membranes for its activity,[31] yet TORC1 also phosphorylates Fab1 (Figure 2). We therefore asked if phosphorylation of Fab1 as probed by our *fab1* alleles would also affect TORC1 activity.

To test for TORC1 activity, we used growth on rapamycin as a readout. Strikingly, we observed that cells carrying *fab1*[6D] grew as poorly as *tor1*Δ cells. In contrast, cells with *fab1*[6A] were slightly more resistant to rapamycin than wild-type cells when grown at either 30°C or 37°C (Figure 4A). All cells grew similarly well in the absence of rapamycin. To reveal if *tor1*Δ and *fab1*[6D] strains differ, we compared their sensitivity on plates containing increasing amounts of rapamycin and observed that *tor1*Δ cells already showed growth deficiency at 1 ng/mL, whereas *fab1*[6D] strains began to show this phenotype at 4 ng/mL (Figure S2A). This indicates that Fab1 mutants modulate TORC1 activity rather than abolish it. When we transformed these cells with a vector encoding wild-type Fab1, we observed rescue of the growth

phenotypes on rapamycin (Figure 4B). This indicates that the mutations did not cause secondary defects within the genome and that the Fab1 mutant alleles are not dominant over the wild-type allele. We conclude that Fab1 phosphorylation also affects TORC1 activity.

To determine if Fab1 phosphorylation specifically affects TORC1 activity on endosomes or vacuoles (Figure 4C), we used established TORC1 activity reporters that specifically localize to endosomes (ET) or to vacuoles (VT)[47,52] (see STAR Methods; Figure 4D). We determined TORC1 activity by decorating blots with a phospho-specific antibody to Sch9, which recognizes phosphorylated Sch9-Thr[737], a bona fide TORC1 target residue in yeast (Figure 4C). By shifting cells from proline to glutamine, TORC1 is strongly activated,[57] as indicated by a strong increase in the phosphorylation signal of both reporters (ET and VT) and endogenous Sch9 (Figure 4C). Both ET and VT reporters behaved similarly in the wild type and *fab1*[6A] mutant. In contrast, their phosphorylation, like that of endogenous Sch9, was strongly impaired in the
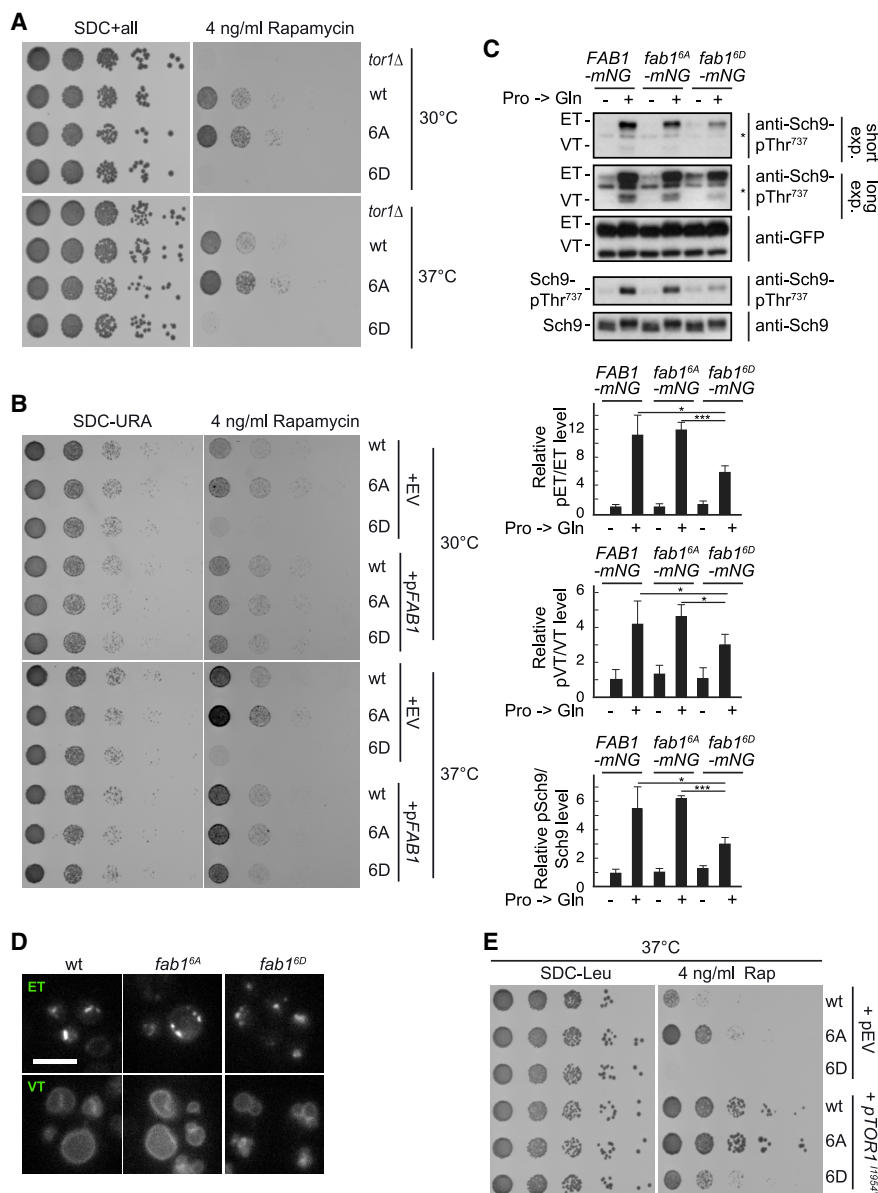
Figure 4. Fab1 Mutations Affect TORC1 Activity

(A) Growth phenotype of *fab1* mutants on rapamycin. The indicated strains were grown to exponential growth phase in SDC+all medium, diluted sequentially 10-fold, spotted onto plates containing SDC+all with or without 4 ng/mL rapamycin, and grown at 30°C or 37°C for 2–5 days.

(B) Complementation of *fab1* mutants. The indicated cells were transformed with an empty vector (EV) or a plasmid encoding wild-type Fab1 (p*FAB1*). The same spotting assay was done as in (A) on the indicated plates.

(C) Expression of the Fab1[6D] allele impairs TORC1 activation at both endosomes and vacuoles. *FAB1-mNG*, *fab1-mNG[6A]*, and *fab1-mNG[6D]* strains were transformed with ET/VT reporters, grown to mid-log phase in proline medium (Pro), and stimulated (+) or not (−) with 3 mM glutamine (Gln) for 2 min. Proteins were extracted, resolved by SDS-PAGE, and the phosphorylation level of ET, VT, and endogenous Sch9 were detected by immunoblotting using phospho-specific anti-Sch9-pThr[737] antibodies. Input levels of ET/VT and endogenous Sch9 were detected with anti-GFP and anti-Sch9 antibodies, respectively. Different exposures are shown to visualize the effects on ET and VT. The asterisks beside the western blot indicate a nonspecific signal. Significance was determined with a two-tailed Student's t test (***p < 0.001; *p < 0.05; ns, no significant difference)

(D) Localization of GFP-tagged endosomal (ET) and vacuolar TORC1 (VT) reporters. Wild-type, *fab1[6A]*, and *fab1[6D]* cells were transformed either with ET or VT and grown to mid-log phase and analyzed by fluorescence microscopy. Scale bar, 5 μm.

(E) Effect of hyperactive TORC1 on growth phenotypes of *fab1* mutants. A plasmid encoding the hyperactive Tor1[I1954V] allele[56] or the empty vector (EV) were transformed into the indicated strains. The spotting assay was done as in (A) on the indicated plates.

See also Figure S2.

fab1[6D] mutant background, suggesting that phosphorylation of Fab1 causes reduced TORC1 activity. Next, we asked if the expression of the hyperactive Tor1[I1954V] allele[56] could suppress this phenotype and observed that it generally conferred some resistance to rapamycin in all strains. Nevertheless, the *fab1*[6D] strain remained significantly more sensitive to rapamycin when compared to the respective *fab1*[6A] and wild-type strains even in the presence of the Tor1[I1954V] allele (Figure 4E). This suggests that *fab1*[6D] mutant is dominant over known hyperactive mutant alleles of *tor1*. Thus, phosphorylation of Fab1 seems to control TORC1 activity possibly by regulating PI(3,5)P$_2$ synthesis.

TORC1 Controls Local Synthesis of PI(3,5)P$_2$ at the Signaling Endosome

Our data so far imply that TORC1-mediated phosphorylation shifts a significant amount of Fab1 to signaling endosomes. As

Fab1 is a lipid kinase, we wondered if Fab1 would then generate PI(3,5)P$_2$ at signaling endosomes. To determine the local PI(3,5)P$_2$ pools, we searched for a suitable reporter. The S6Kinase homolog Sch9 is a TORC1 target that localizes to vacuoles in a Fab1- and thus PI(3,5)P$_2$-dependent manner, and its N-terminal region (residues 1–390) directly interacts with PI(3,5)P$_2$ *in vitro*.[31] To identify a minimal PI(3,5)P$_2$-interacting fragment within Sch9, we localized several truncations in wild-type cells as GFP-fusion proteins. Whereas full-length GFP-Sch9 and an internally truncated GFP-Sch9[Δ184–397] protein were found in part at the vacuole, all fragments lacking the first 183 residues were cytosolic (Figure 5A). However, GFP-tagged Sch9[1–397], and to a greater extent Sch9[1–183], localized strongly to perivacuolar dots and faintly to vacuoles (Figure 5B). This dot localization was completely lost in mutants lacking Fab1, Vac7 or Vac14, showing that its localization requires PI(3,5)P$_2$ synthesis
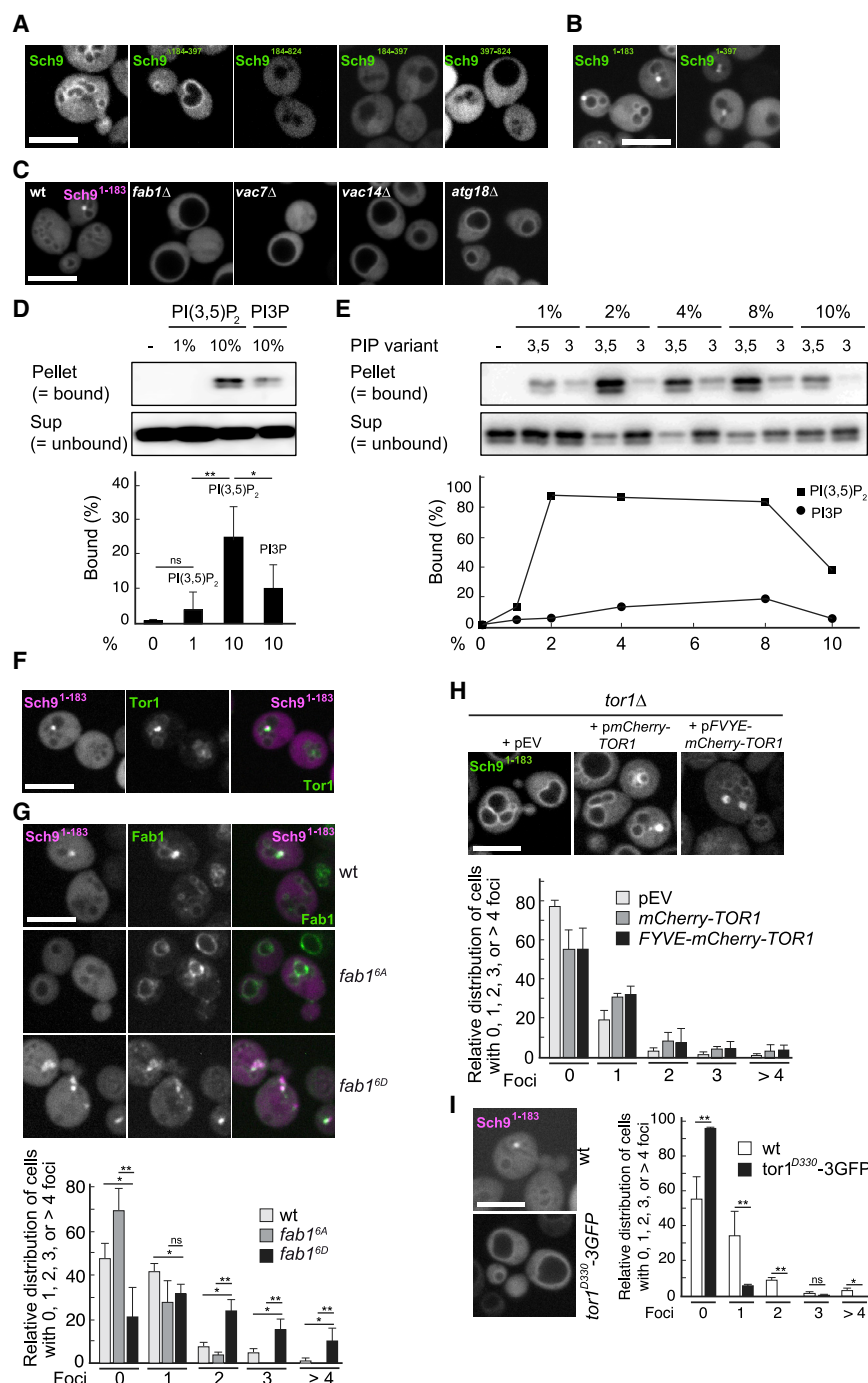
Figure 5. PI(3,5)P$_2$ Production Occurs at Signaling Endosomes

(A–C) Identification of a Sch9 fragment as a PI(3,5)P$_2$ specific reporter.

(A and B) Mapping of Sch9 localization. GFP-tagged Sch9 fragments were expressed in cells, grown to mid-log phase, and localized by fluorescence microscopy. Scale bar, 5 μm.

(C) Localization of the Sch9 fragment, Sch9$^{1-183}$, in mutants of the Fab1 complex. A vector encoding mCherry-tagged Sch9$^{1-183}$ was expressed in wild-type, $fab1\Delta$, $vac7\Delta$, and $vac14\Delta$ cells that were grown to mid-log phase, and Sch9$^{1-183}$ was localized by fluorescence microscopy. Scale bar, 5 μm.

(D and E) Recombinant Sch9$^{1-183}$ binds preferentially to PI(3,5)P$_2$. Liposomes (see STAR Methods) containing the indicated amounts of PI(3,5)P$_2$ and PI3P were incubated with purified His-tagged Sch9$^{1-183}$ and then separated by centrifugation into pellet and supernatant (sup) fractions. Proteins were precipitated by TCA, washed with acetone, dissolved in sample buffer, and resolved on SDS gels and blotted. Western blots were decorated with anti-His antibodies. In (D), liposomes contained 10% PIPs (n = 4), and in (E), different concentrations on liposomes were compared. For details see STAR Methods. Significance was determined with a two-tailed Student's t test (**p < 0.01; *p < 0.05; ns, no significant difference).

(F) Localization of Sch9$^{1-183}$ relative to Tor1. GFP-Tor1 was expressed together with mCherry-tagged Sch9$^{1-183}$ and analyzed as before.

(G) Localization of Sch9$^{1-183}$ in $fab1$ mutants. Cells expressing Fab1-mNeonGreen and corresponding mutants (Figure 3A) were transformed with a plasmid encoding mCherry-tagged Sch9$^{1-183}$ and analyzed as before. Quantification of Sch9 foci/cell is shown below. At least 80 cells were analyzed. Significance was determined with a two-tailed Student's t test (**p < 0.01; *p < 0.05; ns, no significant difference).

(H) Effect of TORC1 localization on Sch9 dot formation. $tor1\Delta$ cells were transformed with the indicated plasmids and GFP-tagged Sch9$^{1-183}$ and analyzed by fluorescence microscopy. For quantification, at least 100 cells were analyzed.

(I) Localization of mCherry-Sch9$^{1-183}$ in $tor1^{D330}$-3GFP cells, in which Tor1 is almost exclusively localized on vacuolar membranes.[47,58] For quantification, at least 100 cells were analyzed. Significance was determined with a two-tailed Student's t test (**p < 0.01; *p < 0.05; ns, no significant difference).

(Figure 5C). Of note, Sch9$^{1-183}$ exclusively decorated vacuoles in $atg18\Delta$ cells, suggesting that Atg18 is required to shift PI(3,5)P$_2$ synthesis from vacuoles to perivacuolar dots, which will be followed up elsewhere.

To confirm the specificity of our probe, we isolated recombinant Sch9$^{1-183}$ from bacteria and incubated the protein with liposomes containing PI3P or PI(3,5)P$_2$ and separated liposomes from proteins by centrifugation. At 10 mol% PI-lipids (Figure 5D), but even more so at lower concentrations, Sch9$^{1-183}$ strongly

accumulated in the pellet fraction of liposomes carrying PI(3,5)P$_2$ (Figure 5E). We therefore used Sch9$^{1-183}$ in further experiments as a reporter of local PI(3,5)P$_2$ levels at vacuoles and endosomes.

To determine if increased PI(3,5)P$_2$ levels are present at signaling endosomes, we analyzed the localization of mCherry-tagged Sch9$^{1-183}$ relative to GFP-Tor1, which is also present on signaling endosomes.[47] Indeed, we found both GFP-Tor1 and mCherry-tagged Sch9$^{1-183}$ in the same dot-like structure

(Figure 5F). A pool of Fab1-GFP was likewise found in mCherry-Sch9$^{1-183}$ positive dots in wild-type cells. These Sch9$^{1-183}$-positive dots increased in size in the *fab1^{6D}* mutant but were reduced in the *fab1^{6A}* mutant (Figure 5G), suggesting that phosphorylation of Fab1 determines also local synthesis of PI(3,5)P$_2$ at the signaling endosome.

As TORC1-mediated phosphorylation results in Fab1 accumulation at signaling endosomes, we next asked whether TORC1 localization also affects endosomal PI(3,5)P$_2$ levels. To alter TORC1 localization, we fused TORC1 to the PI3P-specific FYVE domain of EEA1, which targets TORC1 to endosomes,[47] and still observed mCherry-Sch9$^{1-183}$ in dots (Figure 5H). In turn, we also expressed mCherry-Sch9$^{1-183}$ in a strain expressing Tor1 with three internal GFP-tags, which due to its tagging is found exclusively at the vacuole.[44,47,58] Here, mCherry-Sch9$^{1-183}$ was to a large extent lost from membranes similar to its localization in the *fab1^{6A}* mutant (Figure 5I). These data indicate that endosomal TORC1 is required to maintain a pool of active Fab1 kinase at signaling endosomes, although we do not exclude the possibility that TORC1 regulates Fab1 at the vacuole as well.

Given that TORC1 has multiple targets apart from Fab1 at the signaling endosome and vacuole, we asked if inactivation of TORC1 reverses the aberrant vacuole morphology of the *fab1^{6D}* mutant. We therefore monitored the vacuole morphology of wild-type and *fab1* mutant cells after addition of rapamycin (Figure S2B). Whereas wild-type and the *fab1^{6A}* mutant cells did not show any change in their vacuole morphology, vacuoles of the *fab1^{6D}* mutant became less fragmented (Figures S2B and S2C). This indicates that the vacuole morphology observed in the Fab1 mutant cells is caused by active TORC1.

In summary, we observe that TORC1-mediated phosphorylation of Fab1 causes re-localization of a pool of Fab1 and subsequent local PI(3,5)P$_2$ synthesis at signaling endosomes.

Phosphorylation of Fab1 Determines Its FYVE-Dependent Localization

How could phosphorylation alter the localization of Fab1? Intriguingly, the identified TORC1 phosphorylation sites (S204, 206, 208) are just 20 residues upstream of the FYVE domain of Fab1, a known PI3P interacting domain, which is localized in Fab1 between residues 230 and 320. To test if phosphorylation targets Fab1 via its FYVE domain to PI3P positive endosomes, we deleted the N-terminal 211 residues preceding the FYVE domain. Surprisingly, the *fab1$^{\Delta1-211}$* then behaved like the *fab1^{6D}* mutant. Cells had multiple fragmented vacuoles (Figure 6A), Fab1$^{\Delta1-211}$-positive dots colocalized with Vps8-positive endosomes (Figure 6A), and cells were sensitive to rapamycin (Figure 6C). More Fab1 dots were found in *fab1^{6D}* and Fab1$^{\Delta1-211}$ mutant (Figure 6B). In agreement, the isolated Fab1 FYVE domain interacted specifically with liposomes carrying PI3P, though not as tightly as the isolated PX-domain of the SNARE Vam7 (Figure 6D).

To better understand the N-terminal part of Fab1, we constructed further truncation mutants. Deletions of the first 50 or 100 residues did not affect Fab1 localization and function (Figure S3A and S3B). However, cells expressing Fab1 alleles that were N-terminally truncated for 150 and 190 residues were as sensitive to rapamycin as *fab1$^{\Delta1-211}$* cells (Figure S3B). This

suggests that phosphorylation may relieve an autoinhibition of the FYVE domain and allow its binding to endosomal PI3P. In support of this model, a minimal fragment of the first 330 residues of Fab1 localized to Ivy1-positive endosomes when carrying the phosphomimetic Fab1^{6D} mutations but was found on vacuoles when carrying the Fab1^{6A} mutations (Figure S3C). Interestingly, a Fab1 mutant lacking the entire N-terminal part including the FYVE domain, *fab1$^{\Delta1-320}$*, appeared cytosolic, yet grew like wild type on rapamycin (Figure S3B). This suggests that residual targeting of Fab1 to the vacuole does not require interaction with PI3P, yet may rely on another binding partner on vacuoles. In agreement, cells expressing a point mutant in Fab1 that inactivates the FYVE domain have a slight reduction in cellular PI(3,5)P$_2$ levels and wild-type-like vacuoles, but the mutant Fab1 allele appeared also cytosolic.[11]

Overall, these data show that TORC1-mediated phosphorylation targets a pool of Fab1 via its FYVE domain to endosomes. Phosphorylated Fab1 then generates a local pool of PI(3,5)P$_2$ at signaling endosomes, which in turn recruits more TORC1, and possibly other proteins (Figure S4). Upon fusion of signaling endosomes with vacuoles, the local pool of PI(3,5)P$_2$ may be diluted out and TORC1 and Fab1 may get separated to permit Fab1 dephosphorylation. This circuit may ultimately control both endosomal and vacuolar membrane homeostasis and signaling.

DISCUSSION

This study sheds light on the enigmatic crosstalk between the metabolically regulated TORC1 and the conserved Fab1 lipid kinase complex, which generates the low-abundant lipid PI(3,5)P$_2$.[1,7] In the past, a number of studies unraveled the regulation of Fab1 during osmotic stress, which results in a rapid synthesis of PI(3,5)P$_2$ and subsequent vacuole fragmentation.[11,13,15,16,19,30,59,60] Here, we uncovered that TORC1 phosphorylates Fab1, which in turn controls TORC1 activity. Phosphorylation of Fab1 results in its preferential shift to signaling endosomes, which also accumulate the EGO complex, TORC1, and Ivy1. These structures have been coined vacuolar microdomains in the past,[49,61] yet are clearly endosomes (Figure 1),[47] which lack the ESCRT-III-releasing Vps4 ATPase—as shown here—and thus differ from MVBs. Our data are consistent with the idea that the lipid kinase Fab1 and TORC1 are counter-regulated in space and activity.

We identify an N-terminal part of Fab1, which precedes the PI3P interacting FYVE domain, as a regulator of the Fab1 localization to vacuoles or endosomes. If the N-terminal segment is missing or phosphorylated, Fab1 is found primarily at the signaling endosome. We hypothesize that the FYVE domain is somehow blocked by the N-terminal segment, possibly by folding back to the FYVE domain, creating an autoinhibition. TORC1-mediated phosphorylation of Fab1 could then relieve this block and enable the Fab1 FYVE domain to efficiently bind PI3P at the signaling endosome (Figure S4), a model that requires further testing. Importantly, we observed that signaling endosomes are the main organelles presenting PI(3,5)P$_2$ on their surface, and this lipid may be delivered by fusion to vacuoles, though alternative transport pathways are possible.
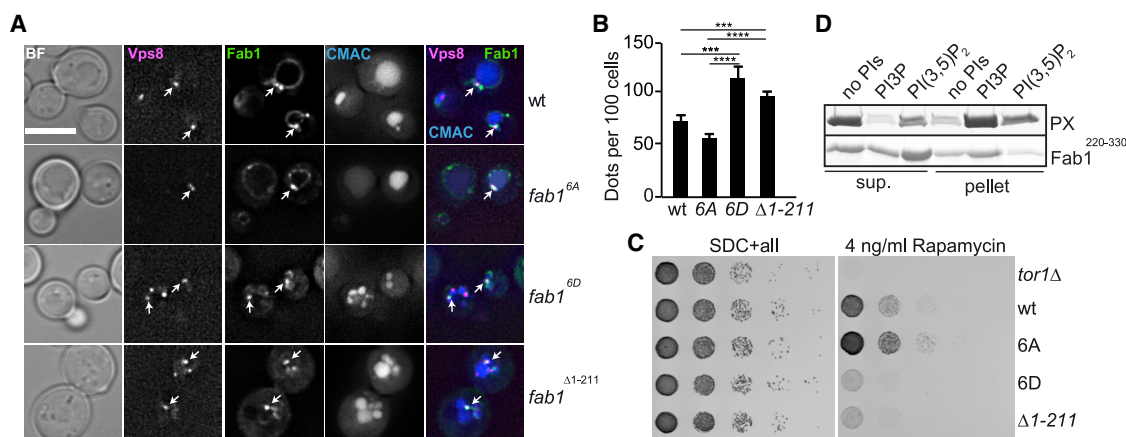
Figure 6. Regulation of Fab1 Targeting to Endosomes by Its FYVE Domain

(A and B) Localization of Fab1 alleles relative to endosomes and vacuoles. The CORVET subunit Vps8 was tagged with mKATE in the indicated strains carrying C-terminally mNEON Green-tagged Fab1. Vacuoles were stained with CMAC. Arrows indicate endosomes. (A) Scale bar, 5 μm. Quantification of dot-like structures is shown in (B). Scale bar, 5 μm. At least 100 cells were counted in three independent experiments. Results are means ± SD. Significance was determined with a two-tailed Student's t test (***p < 0.001; ****p < 0.0001).

(C) Growth of wild-type, *tor1Δ*, and indicated *fab1* mutant strains on rapamycin-containing plates. Spotting of cells was done as before (see Figure 5). wt, wild-type.

(D) Interaction of the Fab1 FYVE domain with liposomes. Liposomes carrying 1 mol% of PI3P, PI(3,5)P_2, or no PIs were incubated with purified PX domain of Vam7 or the Fab1 FYVE domain (residues 230–320), and then separated by centrifugation into pellet and supernatant fraction (see STAR Methods). Proteins were precipitated by TCA, resolved in sample buffer, and analyzed by SDS-PAGE and Coomassie staining.

See also Figures S3 and S4.

The analysis of Fab1 and its metazoan homolog PIKfyve has been challenging as their enzymatic product, PI(3,5)P_2, is a critical lipid for endosome and vacuole/lysosome biogenesis and cellular physiology. Fab1 activity is tightly regulated by intramolecular inhibition,[62] which is relieved in hyperactive alleles[15,59] or by cyclin-dependent kinases (i.e., Pho80/85[63]). Yet, these data could not explain why Fab1 deletions have such an impact on endosomal biogenesis if Fab1 is primarily present on vacuoles.[21] We now consider it likely that this observation is due to an indirect effect on vacuole and endosome biogenesis as PI(3,5)P_2 has multiple effectors at both organelles, including TORC1.

PI(3,5)P_2 recruits TORC1 to vacuoles,[31] and, as we show here, also to signaling endosomes. Specifically, we found TORC1, the TORC1-regulating EGO complex, Ivy1, and Fab1 shift from their primary localization at vacuoles to signaling endosomes in cells expressing the phosphomimetic *fab1*[6D] mutant allele. In such cells, TORC1 activity is significantly reduced on both endosomes and vacuoles and was as reduced as in *tor1Δ* cells. At the vacuole, reduced TORC1 activity could be due to the physical separation of TORC1 from its vacuolar target Sch9. It is also possible that a local excess of PI(3,5)P_2, as observed in the *fab1*[6D] mutant at signaling endosomes, triggers the formation of inactive TORC1 multimers.[44,45] In an intriguing analogy, PI(4,5)P_2 is necessary for TORC2 membrane localization,[64] but spontaneous phase separation of PI(4,5)P_2 into plasma membrane domains sequesters and inactivates TORC2, perhaps also by favoring the formation of inactive TORC2 multimers.[65,66]

We speculate that the lipid kinase and PI3P effector Fab1 and the PI(3,5)P_2 effector TORC1 sense and co-regulate the balance between PI3P and PI(3,5)P_2 at endosomes and at the vacuole. The respective balance of these lipids may locally define the membrane positioning of TORC1 relative to its regulator(s) such as Pib2, which binds PI3P.[40,42,43,45] In addition, the balance between PI3P and PI(3,5)P_2 is likely important for the activity of other PI3P and PI(3,5)P_2 effectors on the vacuole such as the V-ATPase or Atg18.[17,29,30,67]

How could Fab1 and TORC1 sense and regulate the balance between PI3P and PI(3,5)P_2 at endosomes or vacuoles? We propose that the FYVE domain of Fab1 combines two functions: on the one hand, it serves as a sensor for PI3P levels. On the other hand, it functions as a targeting module, which is co-regulated by TORC1-mediated phosphorylation of a stretch of amino acids that is located in its immediate proximity in the N-terminal part of Fab1 (Figure S4). If this stretch is not phosphorylated, it likely auto-inhibits the FYVE domain, which causes Fab1 to primarily localize to the vacuole (Figure S4). On the vacuolar membrane, Fab1 changes the PI3P to PI(3,5)P_2 ratio by consuming PI3P and generating PI(3,5)P_2, which results in enhanced recruitment of TORC1 to the vacuole.

Depending on its metabolic activation state, which is controlled by nutrient cues such as amino acids, TORC1 can then phosphorylate Fab1 proximal to its FYVE domain and thereby release the FYVE domain from autoinhibition (Figure S4). This would then allow the FYVE domain to bind PI3P and consequently favor a redistribution of Fab1 to the signaling endosome, where Fab1 can generate PI(3,5)P_2. In turn, increasing PI(3,5)P_2 will trigger the recruitment of TORC1 to signaling endosomes and hence sequester TORC1 away from its vacuolar targets (Figure S4). As long as TORC1 receives metabolic inputs at signaling endosomes, it will then be able to keep Fab1 phosphorylated in a positive feedback loop. It is likely that phosphorylation of other TORC1 targets is likewise promoted by phosphorylated Fab1 at the signaling endosome and vacuole,[46] which may maintain their identity.

Re-localization of Fab1 to the vacuole (Figure S4) may occur as a results of any of several possible events that are not necessarily mutually exclusive: (1) if TORC1 receives diminished metabolic inputs at the signaling endosome, the autoinhibitory stretch of Fab1 may be preferentially dephosphorylated; (2) Fab1 may consume the majority of the PI3P molecules present on signaling endosomes, thus running out of substrate to associate with; (3) Fab1 is actively dephosphorylated by a yet to be identified phosphatase; or (4) signaling endosomes fuse with vacuoles, thus diluting out PI3P and PI(3,5)P$_2$, separating TORC1 from Fab1, and favoring dephosphorylation of Fab1 as illustrated (Figure S4). In either of these scenarios, Fab1 and TORC1 cooperate in a finely tuned balance. This balance can be affected by superimposed metabolic or osmotic stress control mechanism, which may even differ at the signaling endosome and at the vacuole. In sum, we hypothesize that it is exactly this—the PI3P to PI(3,5)P$_2$ ratio at each organelle—that determines the intimate crosstalk between Fab1 and TORC1.

There are, of course, several open questions. It is intriguing that the PI(3,5)P$_2$ phosphatase Fig4 is part of the Fab1 complex and could also be involved in counterbalancing the Fab1-mediated PI(3,5)P$_2$ synthesis at signaling endosomes or at vacuoles. In addition, the supply routes of PI3P to vacuoles and signaling endosomes likely differ. Vacuoles may receive their PI3P mainly via MVBs, whereas signaling endosomes may perhaps receive PI3P mostly during their biogenesis. Finally, our model may be extended to other vacuolar PI(3,5)P$_2$ effectors, which could be tuned to recognize fine-grained alterations in the respective phosphoinositide levels.

Our model is congruent and supported by all of our observations and compatible with findings of many others in the field. We also suspect that a similar crosstalk extends to metazoans, where the Fab1 homolog PIKfyve also has been linked to mTORC1 activity.[1,22–24] Whether this crosstalk also occurs in metazoans, as shown here for yeast Fab1 and TORC1, is an attractive hypothesis that remains to be evaluated. Intriguingly, the Raptor subunit of mTORC1 also binds PI(3,5)P$_2$, and PIKfyve depletion strongly affects mTORC1 localization in adipocytes.[23] However, PIKfyve depletion has drastic pleiotropic effects on the endolysosomal system. The analysis of a possible mTORC1 and PIKfyve crosstalk will thus require more targeted mutant studies in the future.

PI(3,5)P$_2$ levels are crucial for the correct function of lysosomes, and mutations in subunits of the Fab complex result in neurodegenerative diseases in humans.[25–28] We believe that our novel insights into Fab1-regulation will provide a fresh view on how to understand the origin of these diseases.

STAR★METHODS

Detailed methods are provided in the online version of this paper and include the following:

- KEY RESOURCES TABLE
- RESOURCE AVAILABILITY
  - Lead Contact
  - Materials Availability
  - Data and Code Availability
- EXPERIMENTAL MODEL AND SUBJECT DETAILS
  - Yeast strains, plasmids, and media
- METHOD DETAILS
  - Yeast genetic manipulation and molecular biology
  - Light microscopy and image analysis
  - Growth test
  - *In vivo* local TORC1 activity assay
  - *In vitro* kinase assay of Fab1 fragments with purified TORC1
  - Purification of recombinant Sch9$^{1-183}$-His$_6$
  - Liposome sedimentation assay
  - Mass spectrometry sample preparation and data analysis
- QUANTIFICATION AND STATISTICAL ANALYSIS
  - Co-localization between two proteins
  - Vacuole numbers
  - Dots structures in cells
  - Western blot

AUTHOR CONTRIBUTIONS

Z.C. and P.C.M. conducted all experiments on Fab1 localization and function; R.H. conducted experiments on development and analysis of the Sch9$^{1-183}$ probe; R.N., Z.H., M.-P.P.-G., and J.D. did the phosphorylation assays and analyses; and E.E. and J.W. conceived and performed the initial Sch9 mapping. T.N. and C.J.S. did the lipid analysis of the mutant alleles. J.G. analyzed microcopy data with Z.C. C.D.V. and C.U. conceived the study and wrote the manuscript with support of J.W.

REFERENCES

1. McCartney, A.J., Zhang, Y., and Weisman, L.S. (2014). Phosphatidylinositol 3,5-bisphosphate: low abundance, high significance. BioEssays *36*, 52–64.

2. Balla, T. (2013). Phosphoinositides: tiny lipids with giant impact on cell regulation. Physiol. Rev. *93*, 1019–1137.

3. Adell, M.A.Y., Migliano, S.M., Upadhyayula, S., Bykov, Y.S., Sprenger, S., Pakdel, M., Vogel, G.F., Jih, G., Skillern, W., Behrouzi, R., et al. (2017).

Recruitment dynamics of ESCRT-III and Vps4 to endosomes and implications for reverse membrane budding. eLife 6, e31652.

4. Huotari, J., and Helenius, A. (2011). Endosome maturation. EMBO J. 30, 3481–3500.

5. Schu, P.V., Takegawa, K., Fry, M.J., Stack, J.H., Waterfield, M.D., and Emr, S.D. (1993). Phosphatidylinositol 3-kinase encoded by yeast VPS34 gene essential for protein sorting. Science 260, 88–91.

6. Burd, C., and Cullen, P.J. (2014). Retromer: a master conductor of endosome sorting. Cold Spring Harb. Perspect. Biol. 6, a016774.

7. Hasegawa, J., Strunk, B.S., and Weisman, L.S. (2017). PI5P and PI(3,5)P$_2$: Minor, but Essential Phosphoinositides. Cell Struct. Funct. 42, 49–60.

8. Bonangelino, C.J., Chavez, E.M., and Bonifacino, J.S. (2002). Genomic screen for vacuolar protein sorting genes in Saccharomyces cerevisiae. Mol. Biol. Cell 13, 2486–2501.

9. Weisman, L.S. (2003). Yeast vacuole inheritance and dynamics. Annu. Rev. Genet. 37, 435–460.

10. Michaillat, L., Baars, T.L., and Mayer, A. (2012). Cell-free reconstitution of vacuole membrane fragmentation reveals regulation of vacuole size and number by TORC1. Mol. Biol. Cell 23, 881–895.

11. Botelho, R.J., Efe, J.A., Teis, D., and Emr, S.D. (2008). Assembly of a Fab1 phosphoinositide kinase signaling complex requires the Fig4 phosphoinositide phosphatase. Mol. Biol. Cell 19, 4273–4286.

12. Ho, C.Y., Alghamdi, T.A., and Botelho, R.J. (2012). Phosphatidylinositol-3,5-bisphosphate: no longer the poor PIP2. Traffic 13, 1–8.

13. Jin, N., Chow, C.Y., Liu, L., Zolov, S.N., Bronson, R., Davisson, M., Petersen, J.L., Zhang, Y., Park, S., Duex, J.E., et al. (2008). VAC14 nucleates a protein complex essential for the acute interconversion of PI3P and PI(3,5)P(2) in yeast and mouse. EMBO J. 27, 3221–3234.

14. Alghamdi, T.A., Ho, C.Y., Mrakovic, A., Taylor, D., Mao, D., and Botelho, R.J. (2013). Vac14 protein multimerization is a prerequisite step for Fab1 protein complex assembly and function. J. Biol. Chem. 288, 9363–9372.

15. Gary, J.D., Sato, T.K., Stefan, C.J., Bonangelino, C.J., Weisman, L.S., and Emr, S.D. (2002). Regulation of Fab1 phosphatidylinositol 3-phosphate 5-kinase pathway by Vac7 protein and Fig4, a polyphosphoinositide phosphatase family member. Mol. Biol. Cell 13, 1238–1251.

16. Dove, S.K., Piper, R.C., McEwen, R.K., Yu, J.W., King, M.C., Hughes, D.C., Thuring, J., Holmes, A.B., Cooke, F.T., Michell, R.H., et al. (2004). Svp1p defines a family of phosphatidylinositol 3,5-bisphosphate effectors. EMBO J. 23, 1922–1933.

17. Efe, J.A., Botelho, R.J., and Emr, S.D. (2007). Atg18 regulates organelle morphology and Fab1 kinase activity independent of its membrane recruitment by phosphatidylinositol 3,5-bisphosphate. Mol. Biol. Cell 18, 4232–4244.

18. Bonangelino, C.J., Catlett, N.L., and Weisman, L.S. (1997). Vac7p, a novel vacuolar protein, is required for normal vacuole inheritance and morphology. Mol. Cell. Biol. 17, 6847–6858.

19. Bonangelino, C.J., Nau, J.J., Duex, J.E., Brinkman, M., Wurmser, A.E., Gary, J.D., Emr, S.D., and Weisman, L.S. (2002). Osmotic stress-induced increase of phosphatidylinositol 3,5-bisphosphate requires Vac14p, an activator of the lipid kinase Fab1p. J. Cell Biol. 156, 1015–1028.

20. Dove, S.K., McEwen, R.K., Mayes, A., Hughes, D.C., Beggs, J.D., and Michell, R.H. (2002). Vac14 controls PtdIns(3,5)P(2) synthesis and Fab1-dependent protein trafficking to the multivesicular body. Curr. Biol. 12, 885–893.

21. Odorizzi, G., Babst, M., and Emr, S.D. (1998). Fab1p PtdIns(3)P 5-kinase function essential for protein sorting in the multivesicular body. Cell 95, 847–858.

22. Choy, C.H., Saffi, G., Gray, M.A., Wallace, C., Dayam, R.M., Ou, Z.A., Lenk, G., Puertollano, R., Watkins, S.C., and Botelho, R.J. (2018). Lysosome enlargement during inhibition of the lipid kinase PIKfyve proceeds through lysosome coalescence. J. Cell Sci. 131, jcs213587.

23. Bridges, D., Ma, J.-T., Park, S., Inoki, K., Weisman, L.S., and Saltiel, A.R. (2012). Phosphatidylinositol 3,5-bisphosphate plays a role in the activation and subcellular localization of mechanistic target of rapamycin 1. Mol. Biol. Cell 23, 2955–2962.

24. Zolov, S.N., Bridges, D., Zhang, Y., Lee, W.-W., Riehle, E., Verma, R., Lenk, G.M., Converso-Baran, K., Weide, T., Albin, R.L., et al. (2012). In vivo, Pikfyve generates PI(3,5)P2, which serves as both a signaling lipid and the major precursor for PI5P. Proc. Natl. Acad. Sci. USA 109, 17472–17477.

25. Chow, C.Y., Landers, J.E., Bergren, S.K., Sapp, P.C., Grant, A.E., Jones, J.M., Everett, L., Lenk, G.M., McKenna-Yasek, D.M., Weisman, L.S., et al. (2009). Deleterious variants of FIG4, a phosphoinositide phosphatase, in patients with ALS. Am. J. Hum. Genet. 84, 85–88.

26. Chow, C.Y., Zhang, Y., Dowling, J.J., Jin, N., Adamska, M., Shiga, K., Szigeti, K., Shy, M.E., Li, J., Zhang, X., et al. (2007). Mutation of FIG4 causes neurodegeneration in the pale tremor mouse and patients with CMT4J. Nature 448, 68–72.

27. Lenk, G.M., Ferguson, C.J., Chow, C.Y., Jin, N., Jones, J.M., Grant, A.E., Zolov, S.N., Winters, J.J., Giger, R.J., Dowling, J.J., et al. (2011). Pathogenic mechanism of the FIG4 mutation responsible for Charcot-Marie-Tooth disease CMT4J. PLoS Genet. 7, e1002104.

28. Vaccari, I., Dina, G., Tronchère, H., Kaufman, E., Chicanne, G., Cerri, F., Wrabetz, L., Payrastre, B., Quattrini, A., Weisman, L.S., et al. (2011). Genetic interaction between MTMR2 and FIG4 phospholipid phosphatases involved in Charcot-Marie-Tooth neuropathies. PLoS Genet. 7, e1002319.

29. Gopaldass, N., Fauvet, B., Lashuel, H., Roux, A., and Mayer, A. (2017). Membrane scission driven by the PROPPIN Atg18. EMBO J. 36, 3274–3291.

30. Dove, S.K., Cooke, F.T., Douglas, M.R., Sayers, L.G., Parker, P.J., and Michell, R.H. (1997). Osmotic stress activates phosphatidylinositol-3,5-bisphosphate synthesis. Nature 390, 187–192.

31. Jin, N., Mao, K., Jin, Y., Tevzadze, G., Kauffman, E.J., Park, S., Bridges, D., Loewith, R., Saltiel, A.R., Klionsky, D.J., and Weisman, L.S. (2014). Roles for PI(3,5)P$_2$ in nutrient sensing through TORC1. Mol. Biol. Cell 25, 1171–1185.

32. Dong, X.-P., Shen, D., Wang, X., Dawson, T., Li, X., Zhang, Q., Cheng, X., Zhang, Y., Weisman, L.S., Delling, M., and Xu, H. (2010). PI(3,5)P(2) controls membrane trafficking by direct activation of mucolipin Ca$^{(2+)}$ release channels in the endolysosome. Nat. Commun. 1, 38.

33. Li, S.C., Diakov, T.T., Xu, T., Tarsio, M., Zhu, W., Couoh-Cardel, S., Weisman, L.S., and Kane, P.M. (2014). The signaling lipid PI(3,5)P$_2$ stabilizes V$_1$-V(o) sector interactions and activates the V-ATPase. Mol. Biol. Cell 25, 1251–1262.

34. Loewith, R., and Hall, M.N. (2011). Target of rapamycin (TOR) in nutrient signaling and growth control. Genetics 189, 1177–1201.

35. Thelen, A.M., and Zoncu, R. (2017). Emerging Roles for the Lysosome in Lipid Metabolism. Trends Cell Biol. 27, 833–850.

36. Bar-Peled, L., Chantranupong, L., Cherniack, A.D., Chen, W.W., Ottina, K.A., Grabiner, B.C., Spear, E.D., Carter, S.L., Meyerson, M., and Sabatini, D.M. (2013). A Tumor suppressor complex with GAP activity for the Rag GTPases that signal amino acid sufficiency to mTORC1. Science 340, 1100–1106.

37. Panchaud, N., Péli-Gulli, M.-P., and De Virgilio, C. (2013). SEACing the GAP that nEGOCiates TORC1 activation: evolutionary conservation of Rag GTPase regulation. Cell Cycle 12, 2948–2952.

38. Panchaud, N., Péli-Gulli, M.-P., and De Virgilio, C. (2013). Amino acid deprivation inhibits TORC1 through a GTPase-activating protein complex for the Rag family GTPase Gtr1. Sci. Signal. 6, ra42.

39. Kim, A., and Cunningham, K.W. (2015). A LAPF/phafin1-like protein regulates TORC1 and lysosomal membrane permeabilization in response to endoplasmic reticulum membrane stress. Mol. Biol. Cell 26, 4631–4645.

40. Michel, A.H., Hatakeyama, R., Kimmig, P., Arter, M., Peter, M., Matos, J., De Virgilio, C., and Kornmann, B. (2017). Functional mapping of yeast genomes by saturated transposition. eLife 6, e23570.

41. Tanigawa, M., and Maeda, T. (2017). An *In Vitro* TORC1 Kinase Assay That Recapitulates the Gtr-Independent Glutamine-Responsive TORC1 Activation Mechanism on Yeast Vacuoles. Mol. Cell. Biol. *37*, e00075-17.

42. Ukai, H., Araki, Y., Kira, S., Oikawa, Y., May, A.I., and Noda, T. (2018). Gtr/Ego-independent TORC1 activation is achieved through a glutamine-sensitive interaction with Pib2 on the vacuolar membrane. PLoS Genet. *14*, e1007334.

43. Varlakhanova, N.V., Mihalevic, M.J., Bernstein, K.A., and Ford, M.G.J. (2017). Pib2 and the EGO complex are both required for activation of TORC1. J. Cell Sci. *130*, 3878–3890.

44. Prouteau, M., Desfosses, A., Sieben, C., Bourgoint, C., Lydia Mozaffari, N., Demurtas, D., Mitra, A.K., Guichard, P., Manley, S., and Loewith, R. (2017). TORC1 organized in inhibited domains (TOROIDs) regulate TORC1 activity. Nature *550*, 265–269.

45. Sullivan, A., Wallace, R.L., Wellington, R., Luo, X., and Capaldi, A.P. (2019). Multilayered regulation of TORC1-body formation in budding yeast. Mol. Biol. Cell *30*, 400–410.

46. Hatakeyama, R., and De Virgilio, C. (2019). A spatially and functionally distinct pool of TORC1 defines signaling endosomes in yeast. Autophagy *15*, 915–916.

47. Hatakeyama, R., Péli-Gulli, M.-P., Hu, Z., Jaquenoud, M., Garcia Osuna, G.M., Sardu, A., Dengjel, J., and De Virgilio, C. (2019). Spatially Distinct Pools of TORC1 Balance Protein Homeostasis. Mol. Cell *73*, 325–338.e8.

48. Di Fiore, P.P., and von Zastrow, M. (2014). Endocytosis, signaling, and beyond. Cold Spring Harb. Perspect. Biol. *6*, a016865.

49. Numrich, J., Péli-Gulli, M.-P., Arlt, H., Sardu, A., Griffith, J., Levine, T., Engelbrecht-Vandré, S., Reggiori, F., De Virgilio, C., and Ungermann, C. (2015). The I-BAR protein Ivy1 is an effector of the Rab7 GTPase Ypt7 involved in vacuole membrane homeostasis. J. Cell Sci. *128*, 2278–2292.

50. Malia, P.C., Numrich, J., Nishimura, T., González Montoro, A., Stefan, C.J., and Ungermann, C. (2018). Control of vacuole membrane homeostasis by a resident PI-3,5-kinase inhibitor. Proc. Natl. Acad. Sci. USA *115*, 4684–4689.

51. Varlakhanova, N.V., Tornabene, B.A., and Ford, M.G.J. (2018). Ivy1 is a negative regulator of Gtr-dependent TORC1 activation. J. Cell Sci. *131*, jcs218305.

52. Hatakeyama, R., and De Virgilio, C. (2019). TORC1 specifically inhibits microautophagy through ESCRT-0. Curr. Genet. *65*, 1243–1249.

53. Urban, J., Soulard, A., Huber, A., Lippman, S., Mukhopadhyay, D., Deloche, O., Wanke, V., Anrather, D., Ammerer, G., Riezman, H., et al. (2007). Sch9 is a major target of TORC1 in *Saccharomyces cerevisiae*. Mol. Cell *26*, 663–674.

54. Brunn, G.J., Williams, J., Sabers, C., Wiederrecht, G., Lawrence, J.C., Jr., and Abraham, R.T. (1996). Direct inhibition of the signaling functions of the mammalian target of rapamycin by the phosphoinositide 3-kinase inhibitors, wortmannin and LY294002. EMBO J. *15*, 5256–5267.

55. Reggiori, F., Black, M.W., and Pelham, H.R. (2000). Polar transmembrane domains target proteins to the interior of the yeast vacuole. Mol. Biol. Cell *11*, 3737–3749.

56. Reinke, A., Chen, J.C.-Y., Aronova, S., and Powers, T. (2006). Caffeine targets TOR complex I and provides evidence for a regulatory link between the FRB and kinase domains of Tor1p. J. Biol. Chem. *281*, 31616–31626.

57. Stracka, D., Jozefczuk, S., Rudroff, F., Sauer, U., and Hall, M.N. (2014). Nitrogen source activates TOR (target of rapamycin) complex 1 via glutamine and independently of Gtr/Rag proteins. J. Biol. Chem. *289*, 25010–25020.

58. Sturgill, T.W., Cohen, A., Diefenbacher, M., Trautwein, M., Martin, D.E., and Hall, M.N. (2008). TOR1 and TOR2 have distinct locations in live cells. Eukaryot. Cell *7*, 1819–1830.

59. Duex, J.E., Tang, F., and Weisman, L.S. (2006). The Vac14p-Fig4p complex acts independently of Vac7p and couples PI3,5P2 synthesis and turnover. J. Cell Biol. *172*, 693–704.

60. Rudge, S.A., Anderson, D.M., and Emr, S.D. (2004). Vacuole size control: regulation of PtdIns(3,5)P2 levels by the vacuole-associated Vac14-Fig4 complex, a PtdIns(3,5)P$_2$-specific phosphatase. Mol. Biol. Cell *15*, 24–36.

61. Takeda, E., Jin, N., Itakura, E., Kira, S., Kamada, Y., Weisman, L.S., Noda, T., and Matsuura, A. (2018). Vacuole-mediated selective regulation of TORC1-Sch9 signaling following oxidative stress. Mol. Biol. Cell *29*, 510–522.

62. Lang, M.J., Strunk, B.S., Azad, N., Petersen, J.L., and Weisman, L.S. (2017). An intramolecular interaction within the lipid kinase Fab1 regulates cellular phosphatidylinositol 3,5-bisphosphate lipid levels. Mol. Biol. Cell *28*, 858–864.

63. Jin, N., Jin, Y., and Weisman, L.S. (2017). Early protection to stress mediated by CDK-dependent PI3,5P$_2$ signaling from the vacuole/lysosome. J. Cell Biol. *216*, 2075–2090.

64. Berchtold, D., and Walther, T.C. (2009). TORC2 plasma membrane localization is essential for cell viability and restricted to a distinct domain. Mol. Biol. Cell *20*, 1565–1575.

65. Riggi, M., Kusmider, B., and Loewith, R. (2020). The flipside of the TOR coin - TORC2 and plasma membrane homeostasis at a glance. J. Cell Sci. *133*, jcs242040.

66. Riggi, M., Niewola-Staszkowska, K., Chiaruttini, N., Colom, A., Kusmider, B., Mercier, V., Soleimanpour, S., Stahl, M., Matile, S., Roux, A., and Loewith, R. (2018). Decrease in plasma membrane tension triggers PtdIns(4,5)P$_2$ phase separation to inactivate TORC2. Nat. Cell Biol. *20*, 1043–1051.

67. Banerjee, S., Clapp, K., Tarsio, M., and Kane, P.M. (2019). Interaction of the late endo-lysosomal lipid PI(3,5)P$_2$ with the Vph1 isoform of yeast V-ATPase increases its activity and cellular stress tolerance. J. Biol. Chem. *294*, 9161–9171.

68. Horvath, A., Sütterlin, C., Manning-Krieg, U., Movva, N.R., and Riezman, H. (1994). Ceramide synthesis enhances transport of GPI-anchored proteins to the Golgi apparatus in yeast. EMBO J. *13*, 3687–3695.

69. Brachmann, C.B., Davies, A., Cost, G.J., Caputo, E., Li, J., Hieter, P., and Boeke, J.D. (1998). Designer deletion strains derived from Saccharomyces cerevisiae S288C: a useful set of strains and plasmids for PCR-mediated gene disruption and other applications. Yeast *14*, 115–132.

70. Heitman, J., Movva, N.R., and Hall, M.N. (1991). Targets for cell cycle arrest by the immunosuppressant rapamycin in yeast. Science *253*, 905–909.

71. Binda, M., Péli-Gulli, M.-P., Bonfils, G., Panchaud, N., Urban, J., Sturgill, T.W., Loewith, R., and De Virgilio, C. (2009). The Vam6 GEF controls TORC1 by activating the EGO complex. Mol. Cell *35*, 563–573.

72. Takatori, S., Tatematsu, T., Cheng, J., Matsumoto, J., Akano, T., and Fujimoto, T. (2016). Phosphatidylinositol 3,5-Bisphosphate-Rich Membrane Domains in Endosomes and Lysosomes. Traffic *17*, 154–167.

73. Sikorski, R.S., and Hieter, P. (1989). A system of shuttle vectors and yeast host strains designed for efficient manipulation of DNA in *Saccharomyces cerevisiae*. Genetics *122*, 19–27.

74. Generoso, W.C., Gottardi, M., Oreb, M., and Boles, E. (2016). Simplified CRISPR-Cas genome editing for *Saccharomyces cerevisiae*. J. Microbiol. Methods *127*, 203–205.

75. Janke, C., Magiera, M.M., Rathfelder, N., Taxis, C., Reber, S., Maekawa, H., Moreno-Borchart, A., Doenges, G., Schwob, E., Schiebel, E., and Knop, M. (2004). A versatile toolbox for PCR-based tagging of yeast genes: new fluorescent proteins, more markers and promoter substitution cassettes. Yeast *21*, 947–962.

76. Longtine, M.S., McKenzie, A., 3rd, Demarini, D.J., Shah, N.G., Wach, A., Brachat, A., Philippsen, P., and Pringle, J.R. (1998). Additional modules for versatile and economical PCR-based gene deletion and modification in *Saccharomyces cerevisiae*. Yeast *14*, 953–961.

77. LaGrassa, T.J., and Ungermann, C. (2005). The vacuolar kinase Yck3 maintains organelle fragmentation by regulating the HOPS tethering complex. J. Cell Biol. *168*, 401–414.

78. Péli-Gulli, M.-P., Raucci, S., Hu, Z., Dengjel, J., and De Virgilio, C. (2017). Feedback Inhibition of the Rag GTPase GAP Complex Lst4-Lst7 Safeguards TORC1 from Hyperactivation by Amino Acid Signals. Cell Rep. 20, 281–288.

79. Zech, R., Kiontke, S., Mueller, U., Oeckinghaus, A., and Kümmel, D. (2016). Structure of the Tuberous Sclerosis Complex 2 (TSC2) N Terminus Provides Insight into Complex Assembly and Tuberous Sclerosis Pathogenesis. J. Biol. Chem. 291, 20008–20020.

80. Zarei, M., Sprenger, A., Rackiewicz, M., and Dengjel, J. (2016). Fast and easy phosphopeptide fractionation by combinatorial ERLIC-SCX solid-phase extraction for in-depth phosphoproteome analysis. Nat. Protoc. 11, 37–45.

81. Cox, J., and Mann, M. (2008). MaxQuant enables high peptide identification rates, individualized p.p.b.-range mass accuracies and proteome-wide protein quantification. Nat. Biotechnol. 26, 1367–1372.

82. Tyanova, S., Temu, T., Sinitcyn, P., Carlson, A., Hein, M.Y., Geiger, T., Mann, M., and Cox, J. (2016). The Perseus computational platform for comprehensive analysis of (prote)omics data. Nat. Methods 13, 731–740.

STAR★METHODS

KEY RESOURCES TABLE

REAGENT or RESOURCE	SOURCE	IDENTIFIER
Antibodies		
Rabbit anti-CPY	Horvath et al.[68]	N/A
Rabbit anti-Pgk1	Fulvio Reggiori	N/A
Goat anti-Sch9	De Virgilio lab	N/A
Rabbit anti-Sch9-pThr[737]	De Virgilio lab	N/A
Mouse Monoclonal anti-GFP	Roche	118144600001; RRID: AB_390913
Mouse Monnoclonal anti-HIS tag	SIGMA-ALDRICH	SAB1305538
Bacterial and Virus Strains		
DH5α Competent Cells	Invitrogen	Cat#18265017
Rosetta™(DE3) Competent Cells	Novagen	Cat#70954
Chemicals, Peptides, and Recombinant Proteins		
Rapamycin	LC Laboratories	Cat#R-5000
Wortmannin	LC Laboratories	Cat#W-2990
G418 (Geneticin)	Carl Roth GmbH	Art. No. 2039.3 CAS: 108321-42-2
Hygromycin B	Carl Roth GmbH	Art. No. 1287.2 CAS: 31282-04-9
Nourseothricin (clonNAT)	Jena Bioscience	CAS: 96736-11-7
Ampicillin sodium salt	Carl Roth GmbH	Art. No. K029.2 CAS: 69-52-3
Kanamycin	Carl Roth GmbH	Art. No. T832.3 CAS: 25389-94-0
Cycloheximide	Applichem	Cat#10020730
30% Acrylamide/Bis Solution, 37.5:1	Carl Roth GmbH	Art.Nr. 3029.1
Pefabloc® SC-Protease-Inhibitor	Carl Roth GmbH	Art.Nr. A154.1 CAS: 30827-99-7
Pepstatin A	Carl Roth GmbH	Art.Nr. 2936.2 CAS: 26305-03-3
Leupeptin	Roche	Cat#1017101
1,10-Phenanthroline 1-hydrate	PanReac AppliChem ITW Reagents	13132; CAS: 5144-89-8
Phenylmethyl sulphonyl fluoride	Carl Roth GmbH	Art.Nr. 6367.2
CHAPS	Carl Roth GmbH	Art.Nr. 149.2
EDTA Disodium Salt 2-hydrate	PanReac AppliChem ITW Reagents	A2937; CAS: 6381-92-6
DTT	PanReac AppliChem ITW Reagents	A1101; CAS: 3483-12-3
Tris	PanReac AppliChem ITW Reagents	A1379; CAS: 77-86-1
Glycerol	Carl Roth GmbH	Art. No. 7530.4 CAS: 56-81-5
Imidazole	Carl Roth GmbH	Art. No. X998.4 CAS: 288-32-4
CSM(powder)	MP Biomedicals	SKU: 114500022
CSM-Ura(powder)	MP Biomedicals	SKU 114511212
18:1 (Δ9-Cis) PC (DOPC)	Avanti Polar Lipids	SKU: 850375P
18:1 (Δ9-Cis) PE (DOPE)	Avanti Polar Lipids	SKU: 850725P

(Continued on next page)

Continued

REAGENT or RESOURCE	SOURCE	IDENTIFIER
PI(3)P diC16	Echelon Bioscience	SKU: P-3016-
PI(3,5)P2 diC16	Echelon Bioscience	SKU: P-3516-
ATTO-DPPE dye	ATTO-TEC	AD550-151
CellTracker Blue CMAC Dye	Invitrogen	Cat#C2110
FM™ 4-64 Dye	Invitrogen	Cat#T3166
Coomassie® Brilliant blue G-250	PanReac AppliChem ITW Reagents	A3480; CAS: 6104-58-1
Glutathione Sepharose® 4B	Merck	SKU: GE17-0756-01
Protino™ Ni-NTA Agarose	Macherey-Nagel	CAS: 64-17-5
Dynabeads M-270 Epoxy	Thermo Fisher	Cat#14304
$[\gamma\text{-}^{32}P]$-ATP	Hartmann Analytic	Cat#SRP-501
Sypro® Ruby Protein Gel Stain	Merck	Cat#S4942
Arg10	Cambridge Isotope Laboratories	CNLM-539-H
Lys8	Cambridge Isotope Laboratories	CNLM-291-H
10kD MW-cutoff filters	PALL	OD030C34
Titanium dioxide	GL Sciences	5020-75010
Critical Commercial Assays		
NucleoSpin Gel and PCR Clean-up	Macherey-Nagel	REF 740609.250
GeneJET™ Plasmid-Miniprep-Kit	Thermo Fisher Scientific	Cat#K0503
Experimental Models: Cell Lines		
S. cerevisiae: Strain background: BY4741	Brachmann et al.[69]	N/A
S. cerevisiae: Strain background: BY4727	Brachmann et al.[69]	N/A
Experimental Models: Organisms/Strains		
CUY518: MATa; *his3Δ1, leu2Δ0, met15Δ0, ura3Δ0 tor1Δ::KanMX*	Heitman et al.[70]	N/A
CUY10936: MATa; *his3Δ1, leu2Δ0, met15Δ0, ura3Δ0 FAB1::mNeonGreen::hphNT1*	This study	N/A
CUY11107: MATα ; *his3Δ200 leu2Δ0 lys2Δ0 met15Δ0 trp1Δ63 ura3Δ0 FAB1::VC::KanMX*	This study	N/A
CUY11172: MATa; *his3Δ1, leu2Δ0, met15Δ0, ura3Δ0 FAB1::mNeonGreen::hphNT1 ADH1pr-mCherry:: KOG1*	This study	N/A
CUY11260: MATα ; *his3Δ200 leu2Δ0 lys2Δ0 met15Δ0 trp1Δ63 ura3Δ0 FAB1::VC::KanMX TRP1::CET1pr-VN::KOG1*	This study	N/A
CUY11579: MATa; *his3Δ1, leu2Δ0, met15Δ0, ura3Δ0 FAB1::mNeonGreen::hphNT1 VPS8::mKate::ClonNAT*	This study	N/A
CUY11710: MATa; *his3Δ1, leu2Δ0, met15Δ0, ura3Δ0 IVY1::GFP::hphNT1 VPS8:: mKate::ClonNAT*	This study	N/A
CUY11845: MATα ; *his3Δ200 leu2Δ0 lys2Δ0 met15Δ0 trp1Δ63 ura3Δ0 FAB1::VC::Kan MXTRP1::CET1pr-VN::KOG1 VPS8::mkate::ClonNAT*	This study	N/A
CUY11922: MATa; *his3Δ1, leu2Δ0, met15Δ0, ura3Δ0 fab1$^{S202A/S203A/S204A/T206A/S208A/S210A}$::mNeonGreen:: hphNT1*	This study	N/A
CUY11923: MATa; *his3Δ1, leu2Δ0, met15Δ0, ura3Δ0 fab1$^{S202D/S203D/S204D/T206D/S208D/S210D}$::mNeonGreen:: hphNT1*	This study	N/A
CUY11972: MATa; *his3Δ1, leu2Δ0, met15Δ0, ura3Δ0 FAB1::mNeonGreen-hphNT1 IVY1::3xmcherry-ClonNAT*	This study	N/A

Continued

REAGENT or RESOURCE	SOURCE	IDENTIFIER
CUY11973: MATa; *his3Δ1, leu2Δ0, met15Δ0, ura3Δ0 fab1*$^{S202A/S203A/S204A/T206A/S208A/S210A}$*::mNeonGreen:: hphNT1 IVY1::3xmcherry-ClonNAT*	This study	N/A
CUY11974: MATa; *his3Δ1, leu2Δ0, met15Δ0, ura3Δ0 fab1*$^{S202D/S203D/S204D/T206D/S208D/S210D}$*::mNeonGreen:: hphNT1 IVY1::3xmcherry-ClonNAT*	This study	N/A
CUY11976: MATa; *his3Δ1, leu2Δ0, met15Δ0, ura3Δ0 fab1*$^{S202A/S203A/S204A/T206A/S208A/S210A}$*::mNeonGreen:: hphNT1 KOG1::CloNAT-ADHpr*	This study	N/A
CUY11977: MATa; *his3Δ1, leu2Δ0, met15Δ0, ura3Δ0 fab1*$^{S202D/S203D/S204D/T206D/S208D/S210D}$*::mNeonGreen:: hphNT1 KOG1::CloNAT-ADHpr*	This study	N/A
CUY12077: MATa; *his3Δ1, leu2Δ0, met15Δ0, ura3Δ0 fab1*$^{S202A/S203A/S204A/T206A/S208A/S210A}$	This study	N/A
CUY12078: MATa; *his3Δ1, leu2Δ0, met15Δ0, ura3Δ0 fab1*$^{S202D/S203D/S204D/T206D/S208D/S210D}$	This study	N/A
CUY12125: MATα ; *his3Δ200 leu2Δ0 lys2Δ0 met15Δ0 trp1Δ63 ura3Δ0 VPS4::3xHA-mCherry::TRP1 FAB1::mNeonGreen::hphNT1*	This study	N/A
CUY12219: MATa; *his3Δ1, leu2Δ0, met15Δ0, ura3Δ0 EGO1::GFP::hphNT1 CloNAT::ADH1pr-mCherry:: KOG1*	This study	N/A
CUY12220: MATa; *his3Δ1, leu2Δ0, met15Δ0, ura3Δ0 fab1*$^{S202A/S203A/S204A/T206A/S208A/S210A}$ *EGO1::GFP:: hphNT1 CloNAT::ADH1pr-mCherry::KOG1*	This study	N/A
CUY12221: MATa; *his3Δ1, leu2Δ0, met15Δ0, ura3Δ0 fab1*$^{S202D/S203D/S204D/T206D/S208D/S210D}$ *EGO1::GFP:: hphNT1 CloNAT::ADH1pr-mCherry::KOG1*	This study	N/A
CUY12227: MATa; *his3Δ1, leu2Δ0, met15Δ0, ura3Δ0 IVY1::mGFP-hphNT1 VPS4::3xHA-mCherrry-KanMX*	This study	N/A
CUY12259: MATa; *his3Δ1, leu2Δ0, met15Δ0, ura3Δ0 URA3::PHO5pr-GFP::FAB1*	This study	N/A
CUY12260: MATa; *his3Δ1, leu2Δ0, met15Δ0, ura3Δ0 URA3::PHO5pr-GFP::FAB1-211aa-end*	This study	N/A
CUY12341: MATa; *his3Δ1, leu2Δ0, met15Δ0, ura3Δ0 URA3::PHO5pr-GFP:: fab1*$^{S202A/S203A/S204A/T206A/S208A/S210A}$	This study	N/A
CUY12342: MATa; *his3Δ1, leu2Δ0, met15Δ0, ura3Δ0 URA3::PHO5pr-GFP:: fab1*$^{S202D/S203D/S204D/T206D/S208D/S210D}$	This study	N/A
CUY12354: MATa; *his3Δ1, leu2Δ0, met15Δ0, ura3Δ0 URA3::PHO5pr-GFP::FAB1 VPS8:: mKate::hphNT1*	This study	N/A
CUY12355: MATa; *his3Δ1, leu2Δ0, met15Δ0, ura3Δ0 URA3::PHO5pr-GFP::FAB1-211aa-end VPS8:: mKate::hphNT1*	This study	N/A
CUY12356: MATa; *his3Δ1, leu2Δ0, met15Δ0, ura3Δ0 URA3::PHO5pr-GFP:: fab1*$^{S202A/S203A/S204A/T206A/S208A/S210A}$ *VPS8:: mKate::hphNT1*	This study	N/A
CUY12357: MATa; *his3Δ1, leu2Δ0, met15Δ0, ura3Δ0 URA3::PHO5pr-GFP:: fab1*$^{S202D/S203D/S204D/T206D/S208D/S210D}$ *VPS8:: mKate::hphNT1*	This study	N/A
CUY12362: MATa; *his3Δ1, leu2Δ0, met15Δ0, ura3Δ0 URA::PHO5pr-GFP-FAB1-151aa-end*	This study	N/A

Continued

REAGENT or RESOURCE	SOURCE	IDENTIFIER
CUY12365: MATa; *his3Δ1, leu2Δ0, met15Δ0, ura3Δ0 URA::PHO5pr-GFP-FAB1-191aa-end*	This study	N/A
CUY12367: MATa; *his3Δ1, leu2Δ0, met15Δ0, ura3Δ0 URA::PHO5pr-GFP-FAB1-321aa-end*	This study	N/A
CUY12445: MATa; *his3Δ1, leu2Δ0, met15Δ0, ura3Δ0 URA::PHO5pr-GFP-FAB1-51aa-end*	This study	N/A
CUY12446: MATa; *his3Δ1, leu2Δ0, met15Δ0, ura3Δ0 URA::PHO5pr-GFP-FAB1-101aa-end*	This study	N/A
CUY12650: *MATa his3Δ1 leu2Δ0 met15Δ0 ura3Δ0 IVY1::mGFP-hphNT1 KOG1::CloNAT-ADHpr*	This study	N/A
CUY12653: *MATa his3Δ1 leu2Δ0 met15Δ0 ura3Δ0 FAB1::mNeonGreen-hphnt1 VPS4::3xHA-mCherry-KanMX*	This study	N/A
CUY12654: *MATa his3Δ1 leu2Δ0 met15Δ0 ura3Δ0 FAB1 ^{S202A,S203A,S204A,T206A,S208A,S210}:: mNeonGreen-hpHNt1 VPS4::3xHA-mCherry-KanMX*	This study	N/A
CUY12655: *MATa his3Δ1 leu2Δ0 met15Δ0 ura3Δ0 FAB1 ^{S202D,S203D,S204D,T206D,S208D,S210D}:: mNeonGreen-hpHNt1 VPS4::3xHA-mCherry-KanMX*	This study	N/A
CUY12656: *MATalpha his3Δ200 leu2Δ0 lys2Δ0 met15Δ0 trp1Δ63 ura3Δ0 FAB1::VC-KanMX TRP1-CET1pr-VN::KOG1 IVY1::mkate-natNT2*	This study	N/A
YL516: MATa ; *his3Δ1, leu2Δ0, ura3Δ0*	Binda et al.[71]	N/A
RKH395: MATa ; *his3Δ1, leu2Δ0, ura3Δ0 LEU2::GFP-TOR1*	Horvath et al.[68]	N/A
RKH486: MATa ; *leu2Δ0, ura3Δ0 his3Δ1::GFP-SCH9$^{1-183}$::SpHIS5*	This study	N/A
RKH488: MATa ; *leu2Δ0, ura3Δ0 his3Δ1::GFP-SCH9$^{1-183}$::SpHIS5 fab1Δ::KanMX*	This study	N/A
RKH490: MATa ; *leu2Δ0, ura3Δ0 his3Δ1::GFP-SCH9$^{1-183}$::SpHIS5 vac7Δ::KanMX*	This study	N/A
RKH492: MATa ; *leu2Δ0, ura3Δ0 his3Δ1::GFP-SCH9$^{1-183}$::SpHIS5 vac14Δ::KanMX*	This study	N/A
RKH555: MATa ; *leu2Δ0, ura3Δ0 his3Δ1::GFP-SCH9$^{1-183}$::SpHIS5 atg18Δ::KanMX*	This study	N/A
RKH478: MATa ; *his3Δ1, leu2Δ0, ura3Δ0 tor1Δ:: hphNT1 trp1Δ::KanMX*	This study	N/A
MP52-2A: MATa ; *his3Δ1, leu2Δ0, ura3Δ0 tor1^{D330}-3GFP*	Heitman et al.[70]	N/A
Oligonucleotides		
Fab1-Forward GGACAGGGAT GCGGTCAACGAAGAAGgtttta gagctagaaatagcaagttaaaataagg	This study	N/A
Fab1-Reverse CTTCTTCGTTGA CCGCATCCCTGTCCgatcatttat ctttcactgcggag	This study	N/A
HDR-Fab1^{6A} TAAAATGCGAA CAGGAAACTCTTGGcCAGG GcTGCGGcCAACGcAGcAG cGGCACTCTTTATCGAAGA CACTTCATCGCC	This study	N/A
HDR-Fab1^{6D} TAAAATGCGAACAGGAAACTC TTGtcCAGGtcTGCGtcCAAatcAtcAtcGGCAC TCTTTATCGAAGACACTTCATCGCC	This study	N/A

(Continued on next page)

Continued

REAGENT or RESOURCE	SOURCE	IDENTIFIER
Recombinant DNA		
GST-p40-PX	Takatori et al.[72]	N/A
pRS315: *CEN/ARS, LEU2*	Sikorski and Hieter[73]	N/A
pRS413: *CEN/ARS, HIS3*	Sikorski and Hieter[73]	N/A
pRS414: *CEN/ARS, TRP1*	Sikorski and Hieter[73]	N/A
pRS415: *CEN/ARS, LEU2*	Sikorski and Hieter[73]	N/A
pRS416: *CEN/ARS, URA3*	Sikorski and Hieter[73]	N/A
p1379: *CEN/ARS, URA3, MET15*	Hatakeyama and De Virgilio[46]	N/A
p1770: *CEN/ARS, HIS3, MET15*	Varlakhanova et al.[51]	N/A
CU1776: *CEN/ARS, URA3, GFP-CPS1*	Odorizzi et al.[21]	N/A
CU4615: *CEN/ARS, LEU2, 3xHA-TOR1-I1954V*	Stracka et al.[57]	N/A
CU5125: *CEN/ARS, URA3, P_{nop1}-FAB1-1-330aa $^{S202A/S203A/S204A/T206A/S208A/S210A}$-GFP*	This study	N/A
CU5126: *CEN/ARS, URA3, P_{nop1}-FAB1-1-330aa $^{S202D/S203D/S204D/T206D/S208D/S210D}$-GFP*	This study	N/A
CU5263: *CEN/ARS, URA3, P_{nop1}-FAB1-1-330aa-GFP*	This study	N/A
pRCC-K: *2μ, KanMX, Cas9*	Generoso et al.[74]	N/A
CU5048: *2μ, KanMX, Cas9, Fab1-near-203aa*	This study	N/A
p2976: *2μ, URA3, P_{PRC1}-SCH9$^{709-824}$-GFP-PHO8$^{1-63}$*	Hatakeyama and De Virgilio[46]	N/A
p3608: *CEN/ARS, HIS3, P_{VAC8}-yEmRFP-TOR1*	This study	N/A
p3613: *CEN/ARS, HIS3, P_{VAC8}-EEA1(human)$^{1257-1411}$-yEmRFP-TOR1*	This study	N/A
p3693: *CEN/ARS, HIS3, P_{ADH1}-GFP-SCH9$^{1-183}$*	This study	N/A
p3694: *CEN/ARS, HIS3, P_{ADH1}-GFP-SCH9$^{184-397}$*	This study	N/A
p3695: *CEN/ARS, HIS3, P_{ADH1}-GFP-SCH9$^{1-397}$*	This study	N/A
p3715: *CEN/ARS, HIS3, P_{ADH1}-yEmRFP-SCH9$^{1-183}$*	This study	N/A
p3745: *CEN/ARS, HIS3, P_{CYC1}-yEmRFP-SCH9$^{1-183}$*	This study	N/A
p3776: *CEN/ARS, LEU2, P_{CYC1}-GFP-SCH9$^{1-183}$*	This study	N/A
pRH3488: *[pET-28a (+)]-His$_6$-fab1 (1-600) (codon optimized)*	This study	N/A
pRH3490: *[pET-28a (+)]-His$_6$-fab1 (580-1180) (codon optimized)*	This study	N/A
pRH3491: *[pET-28a (+)]-His$_6$-fab1 (1160-1760) (codon optimized)*	This study	N/A
pRH3492: *[pET-28a (+)]-His$_6$-fab1 (1740-2278) (codon optimized)*	This study	N/A
pMP3668: *[pET-28a (+)]-His$_6$-fab1 $^{T206A/ S208A/ S210A}$ (1-600) (3A) (codon optimized)*	This study	N/A
pMP3669: *[pET-28a (+)]-His$_6$-fab1 $^{S203A/ S204A/ T206A/ S208A/ S210A}$ (1-600) (5A) (codon optimized)*	This study	N/A
p2981: *2μ, HIS3, P_{VAC8}-EEA1(human)$^{1257-1411}$-GFP-SCH9$^{709-824}$*	Hatakeyama and De Virgilio[46]	N/A
p3047: *2μ, LEU2, P_{PRC1}-SCH9$^{709-824}$-GFP-PHO8$^{1-63}$*	Hatakeyama and De Virgilio[46]	N/A
pJU793: *CEN/ARS, URA3, GFP-SCH9*	Urban et al.[53]	N/A
p3296: *CEN/ARS, URA3, GFP-SCH9$^{Δ1-183}$*	This study	N/A
p3297: *CEN/ARS, URA3, GFP-SCH9$^{Δ184-397}$*	This study	N/A

Continued

REAGENT or RESOURCE	SOURCE	IDENTIFIER
p3298: *CEN/ARS, URA3, GFP-SCH9*$^{\Delta1-397}$	This study	N/A
p3898: *[pET-24D]-GST-SCH9*$^{1-183}$*-His*$_6$	This study	N/A
pCDF-GP(GST-PreScission)-Fab1-220-330aa	This study	N/A
Software and Algorithms		
Fiji	National Institutes of Health	https://imagej.net/Fiji/Downloads
Adobe Photoshop CS4	Adobe Inc.	N/A
Microsoft Excel	Microsoft Inc.	N/A
GraphPad Prism 8	GraphPad	https://www.graphpad.com/

RESOURCE AVAILABILITY

Lead Contact
Further information and requests for resource and regents should be directed to and will be fulfilled by the Lead Contact, Christian Ungermann (cu@uos.de).

Materials Availability
Yeast strains and plasmids generated in this study are available on request.

Data and Code Availability
The published article includes all datasets generated or analyzed during this study.

EXPERIMENTAL MODEL AND SUBJECT DETAILS

Yeast strains, plasmids, and media
Yeast strains and plasmids are listed in Key Resource table. Yeast strains were grown in yeast extract peptone dextrose (YPD) containing 1% yeast extract, 2% peptone and 2% glucose at 30°C for most growth analyses. For microscopy experiments and spotting assays, yeast strains were grown in synthetic dextrose complete (SDC) media, which contained 6.75 g yeast nitrogen base without amino acids, 20 g glucose, and 0.8 g complete supplement media (CSM) powder per liter.

METHOD DETAILS

Yeast genetic manipulation and molecular biology
S. cerevisiae strains used are listed in Resource Table. Genetic manipulations were made by homologous recombination of PCR fragments as described previously.[75,76] Yeast cells were grown in YPD medium overnight and then diluted to 0.1 OD$_{600}$. They were then grown to log-phase, washed with sterile water, and then with 0.1 M lithium acetate. Cells were resuspended in 350 μl 0.1 M lithium acetate, and 50 μl were used for transformation. The transformation mix contains 240 μl 50% PEG, 36 μl 1 M lithium acetate, 25 μl carrier DNA and 50 μl cells. The mix was incubated at 42°C for 45 min and cells were then plated on selection plates. A CRISPR-Cas9 approach was selected to generate *FAB1* point mutants.[74] For generation of the corresponding Cas9 plasmid (CU5048), the following primers were used: Fw-GGACAGGGATGCGGTCAACGAAGAAGgttttagagctagaaatagcaagttaaaataagg, Rv- CTTCTTCGTTGACCG CATCCCTGTCCgatcatttatctttcactgcggag. We transform both plasmid (CU5048) and the corresponding single stranded DNA (ssDNA) templates for homology directed repair (HDR), HDR-Fab1^{6A} TAAAATGCGAACAGGAAACTCTTGGcCAGGGcTGCGGcC AACGcAGcAGcGGCACTCTTTATCGAAGACACTTCATCGCC) or HDR-Fab1^{6D} (TAAAATGCGAACAGGAAACTCTTGtcCAGGtcTGC GtcCAAatcAtcAtcGGCACTCTTTATCGAAGACACTTCATCGCC), into the used background strains. After transformation, the cells were re-suspended in YPD and grown at 30°C for 1-2 h for recovery before cells were placed onto plates containing G418. Clones containing the correct mutations were identified by sequencing of the *FAB1* region. All plasmids are listed in Resource Table.

Light microscopy and image analysis
Cells were grown to log-phase in yeast extract peptone (YP) medium containing glucose (YPD), or synthetic medium supplemented with essential amino acids (SDC). Vacuole membrane was stained with 30 μM FM4-64 for 30 min, followed by washing with medium, and incubation in medium without dye for 1 h before analysis.[77] For luminal staining of vacuoles, cells were incubated in 0.1 mM 7-amino-4-chloromethylcoumarin (CMAC) for 10 min and washed with SDC medium. Images were acquired on an Olympus IX-71 inverted microscope equipped with a 100x NA 1.49 objective, a sCMOS camara (PCO), an InsightSSI illumination system and SOft-WoRx software (Applied Precision). Images were processed with ImageJ. One representative plane of a z stack is shown unless noted. For quantifications the number of vacuoles were counted in three independent experiments and at least 100 cells were

quantified in each experiment. For determination of colocalization of two proteins, their dot-like signal was quantified as percentage of colocalizing dots.

Growth test

Cells were grown to log-phase, washed twice with SDC, and diluted to an optical density 600 (OD_{600}) of 0.25. Serial dilutions (1:10) were spotted onto plates and imaged after 2-4 days.

In vivo local TORC1 activity assay

Endosomal and vacuolar TORC1 activities were assayed as previously described.[47] The C-terminal portion of Sch9, an established TORC1 substrate, was fused to GFP and an organelle targeting domain: FYVE domain of human EEA1 protein for the endosomal reporter (ET) or the N-terminal domain of Pho8 vacuolar phosphatase for the vacuolar reporter (VT). The strains were transformed with ET/VT reporters and their phosphorylation levels in cell lysate was assessed by western blotting using the phosphospecific anti-Sch9-pThr[737] antibodies.

In vitro kinase assay of Fab1 fragments with purified TORC1

In vitro kinase assays were performed, with some variation, essentially as described.[78] TORC1 was purified from a Tco89-TEV-TAP-expressing yeast strain grown in YPD and treated for 10 min with cycloheximide. The cells were collected by filtration, rapidly frozen in liquid nitrogen, and subjected to cryogenic disruption with an MM 400 Mixer Mill (Retsch). The obtained powder was resuspended in extraction buffer (50 mM HEPES/NaOH, pH 7.5, 5 mM CHAPS, 400 mM NaCl, 1 mM EDTA, 0.5 mM DTT, 400 mM Pefabloc, Roche complete protease inhibitor EDTA-free). The cleared lysate was incubated with IgG-coupled Dynabeads (Dynabeads M-270 Epoxy; Invitrogen) for 2 h at 4°C. After 5 washes with wash buffer (50 mM HEPES/NaOH [pH 7.5], 5 mM CHAPS, 400 mM NaCl, 0.5 mM DTT) the TORC1 complex was eluted using 2% TEV protease and stored at −80°C after addition of 10% glycerol.

Recombinant His$_6$-tagged Fab1 variants were expressed in Rosetta *E. coli* cells. Bacterial cells were disrupted by sonication in lysis buffer (50 mM NaH_2PO_4, pH 8.0, 300 mM NaCl, 10 mM Imidazole, Roche complete protease inhibitor EDTA-free, 0.1% NP40) and proteins were purified through binding to Ni-NTA agarose beads (wash buffer containing 50 mM NaH_2PO_4, pH 8.0, 300 mM NaCl, 20 mM Imidazole; elution buffer containing 50 mM NaH_2PO_4, pH 8.0, 300 mM NaCl, 250 mM Imidazole). Eluted fractions were dialysed into 50 mM HEPES, pH 7.5, 150 mM NaCl, 5% glycerol (Slide-A-Lyzer MINI Dialysis Device, 10K MWCO).

In vitro kinase reactions were performed in kinase buffer (50 mM HEPES/NaOH, pH 7.5, 150 mM NaCl), with 120 ng of purified His$_6$-Fab1 variants and TORC1 (containing 60 ng Tor1) in 30 μl total volume, started by adding the ATP mix (4.2 mM $MgCl_2$, 300 mM ATP, and 3.3 mCi [γ-^{32}P]-ATP [Hartmann Analytic, SRP-501]), and stopped by adding SDS-PAGE sample buffer. Proteins were separated by SDS-PAGE, stained with Sypro Ruby (Sigma) to assess loading, and analyzed using a phosphorimager (Typhoon FLA 9500; GE Healthcare).

Purification of recombinant Sch9$^{1-183}$-His$_6$

GST-Sch9$^{1-183}$-His$_6$, which has a TEV protease cleavage site between the GST and Sch9$^{1-183}$, was purified from bacteria (Rosetta strain). Expression was induced by 0.5 mM IPTG overnight at 18°C. Cells were lysed by sonication in lysis buffer (200 mM NaCl, 50 mM Tris-HCl [pH 7.5], 5% glycerol, 1 mM DTT, Roche protease inhibitor cocktail) and clarified by centrifugation. The protein was purified by incubation with glutathione Sepharose beads for 1 h at 4°C, and washed with lysis buffer. Sch9$^{1-183}$-His$_6$ was eluted by incubating the beads with TEV protease in cleavage buffer (50 mM Tris-HCl [pH 7.5], 0.5 mM EDTA, 1 mM DTT) for 1 h at 30°C.

Liposome sedimentation assay

Liposomes were prepared as previously described[79] with modifications. Liposomes were generated from the lipid mixtures (81.5 mol % dioleoylphosphatidylcholine [Avanti Polar Lipids 850375], 18 mol% dioleoylphosphatidylethanolamine, 0.5 mol% Atto dye [ATTO-TEC AD550-151]) with or without PI(3,5)P_2 or PI3P at the indicated concentrations. The lipids were dried by evaporation for 1 h and dissolved in 1 mL of assay buffer (20 mM PIPES-KOH [pH 6.5], 120 mM KCl) supplemented with 5% w/v sucrose to a final lipid concentration of 2 mM. The liposome suspension was freeze/thawed for 8 times in liquid nitrogen and at 55°C, respectively. For the binding assay, 0.5 μg of Sch9$^{1-183}$-His$_6$ was pre-cleaned in assay buffer by centrifugation at 20,000 g for 20 min at 4°C. The supernatant containing Sch9$^{1-183}$-His$_6$ was mixed with 0.54 mM (final concentration) liposomes and incubated at room temperature for 15 min. The liposomes were then centrifuged (20,000 g for 20 min at 4°C), and the supernatant (unbound fraction) was separated from the pellet (liposome-bound fraction). Samples were TCA-precipitated and analyzed via SDS-PAGE and subsequent immunoblot analysis using the anti-His Tag antibodies (SIGMA-ALDRICH, Germany).

Mass spectrometry sample preparation and data analysis

MS samples were basically generated as described.[47] Briefly, for *in vivo* analyses yeast strains were grown in SILAC medium containing non-labeled or labeled arginine and lysine variants, L-arginine-^{13}C$_6$-^{15}N$_4$ (Arg10) and L-lysine-^{13}C$_6$-^{15}N$_2$ (Lys8) (Sigma-Aldrich). Cells were treated or not with 200 ng/mL rapamycin for 30 min, and trichloroacetic acid (TCA)-treated cell pellets (50 mg) of both labels were mixed, and stored at −80°C for further use. For *in vitro* analyses, purified TORC1 was incubated with the Fab1 (1-600) fragment in the presence of 1 mM $MnCl_2$ for 30 min as described above. As a negative control, purified TORC1 was inhibited with 6 μM wortmannin for 30 min. *In vitro* kinase assays of purified Fab1 variants and TORC1 were performed on 10 kD MW-cutoff filters (Pall) as described.[47]

Proteins were reduced by 1 mM DTT, alkylated by 5 mM iodoacetamide and digested by Lys-C (Lysyl Endopeptidase, WAKO) for 4 h, in case of *in vivo* analyses, and trypsin (Promega) overnight. Phosphopeptides were enriched by TiO_2 beads (GL Sciences) essentially as described[80] and analyzed by LC-MS/MS using a QExactive HF-X mass spectrometer coupled to an EasyLC 1200 nanoflow-HPLC (Thermo Scientific). MS raw files were analyzed using MaxQuant (version 1.6.2.10),[81] and a Uniprot full-length *S.cerevisiae* database (March, 2016) containing common contaminants such as keratins and enzymes used for in-gel digestion. Fixed modification was carbamidomethylcysteine, variable modifications were protein amino-terminal acetylation, serine-, threonine- and tyrosine-phosphorylation, and oxidation of methionine. The MS/MS tolerance was set to 20 ppm and three missed cleavages were allowed using trypsin/P as enzyme specificity. Peptide, site, and protein FDR based on a forward-reverse database were set to 0.01, minimum peptide length was set to 7, the minimum score for modified peptides was 40, and minimum number of peptides for identification of proteins was set to one, which must be unique. MaxQuant results were analyzed using Perseus.[82]

QUANTIFICATION AND STATISTICAL ANALYSIS

Co-localization between two proteins
The number of co-localizing dot-like structure between Fab1 and other proteins (Figures 1C and 3), or Ivy1 (Figure 1A) and other proteins were counted, which were divided by the total numbers of the Fab1 dot-like or Ivy1 dot-like signal. For statistical analysis, two-tailed, unpaired Student's t tests were used, and data is presented as mean + SD.

Vacuole numbers
The number of the cell containing different amounts of vacuoles was counted in Fab1 mutants (Figure 3B). Two-tailed, unpaired Student's t tests were used, and data is presented as mean ± SD.

Dots structures in cells
The number of dot-like signals for each protein were counted per 100 cells, and the results are shown as graphs (Figures 3H and 6B). Two-tailed, unpaired Student's t tests were used, and data is presented as mean + SD. The number of cells containing Sch9[1-183] dots were counted and the relative distribution is shown in Figure 5H (no comparative statistical analysis was performed here) and Figures 5G and 5I (Two-tailed, unpaired Student's t tests were used for statistical analysis).

Western blot
Western blot bands were analyzed by ImageJ, and the quantities were calculated from the relative intensities. For statistical analysis, two-tailed, unpaired Student's t tests were used, and data is presented as mean + SD.